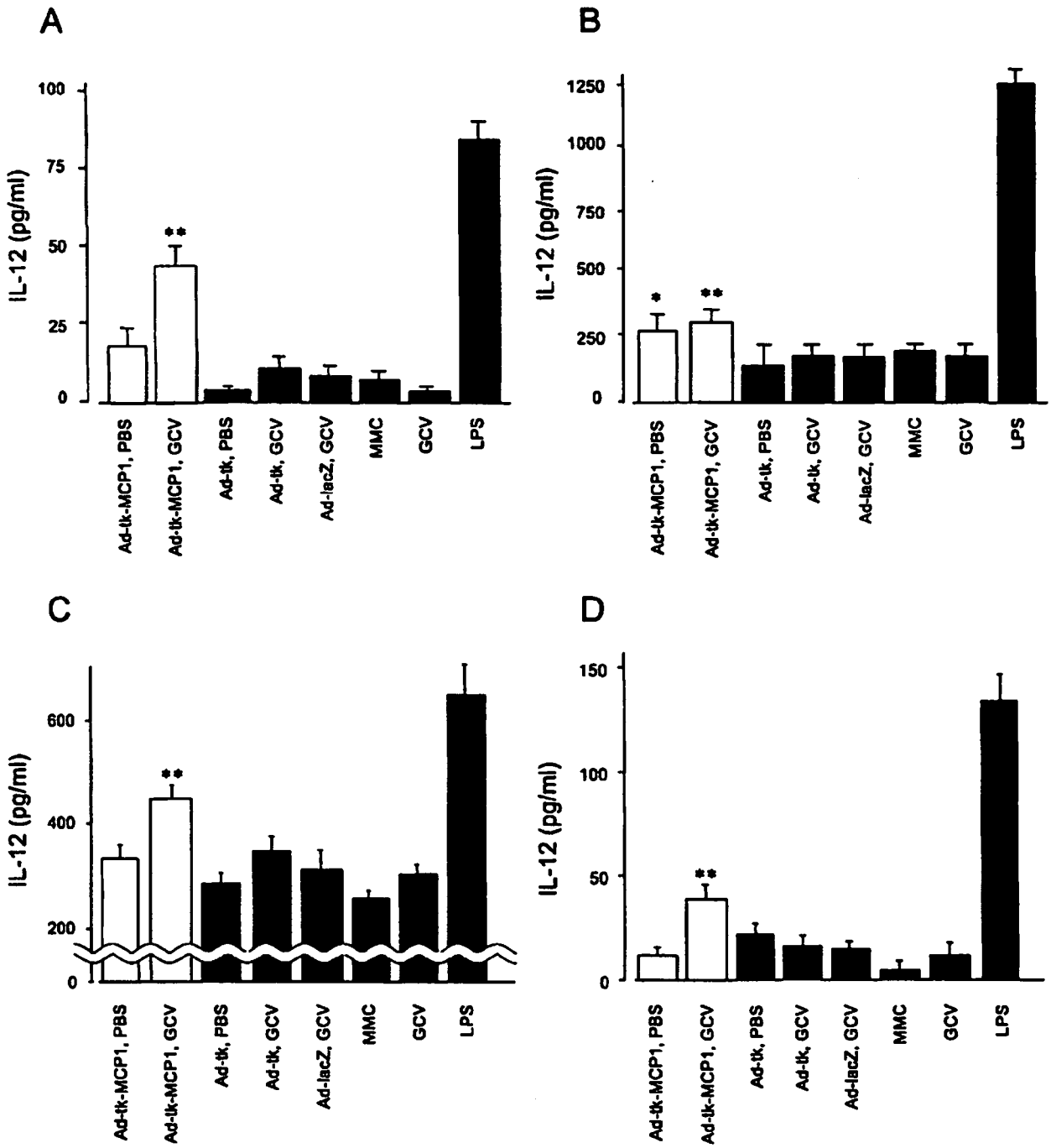

FIGURE 1. IL-12 production by monocytes and DCs cocultured with apoptotic or nonapoptotic HCC cells infected with rAds in vitro. HuH7 cells were infected with Ad-tk-MCP1, Ad-tk, and Ad-lacZ at an MOI of 5 for 24 h. Aliquots of 10^5 mouse (*A*) and human (*C*) monocytes or 10^5 mouse (*B*) and human (*D*) DCs were cocultured with 10^5 rAd- or MMC-treated HuH7 cells and treated with or without GCV for two days, and the concentrations of IL-12 in the medium were evaluated using an immunoassay. Each value is the mean ± SE of triplicate experiments. *, $p < 0.05$ compared to Ad-tk with PBS (Ad-tk, PBS); **, $p < 0.05$ compared to Ad-tk with GCV (Ad-tk, GCV) by the Mann-Whitney *U* test.

Materials and Methods

Recombinant adenoviruses

The bicistronic Ad-tk-MCP1 (10), which harbors the HSV-tk gene and the human MCP-1 gene in sequence and is driven by a CAG promoter constructed from a cytomegalovirus enhancer, a chicken β-actin promoter and part of rabbit β-globin, was prepared, purified, and titrated according to the protocols supplied by the manufacturer (Takara Bio) as described (17, 18). Briefly, using the internal ribosomal entry site (IRES) fragment of the encephalomyocarditis virus, the plasmid ptk-IRES-MCP1 (tk-MCP1) was constructed and the fragment was inserted into the cosmid vector (pAd-tk-MCP1). Ad-tk-MCP1 was subsequently generated by transfecting 293 cells with pAd-tk-MCP1 and *Eco*T22I-digested adenovirus 5-dlX DNA-terminal protein complex. The rAd expressing HSV-tk (Ad-tk), lacZ (Ad-lacZ) and MCP-1 (Ad-MCP1) were constructed in the same way (8). The rAds were purified on cesium gradients and their titers were determined by the 50% tissue culture infectious dose ($TCID_{50}$) method (19).

Cell lines and culture

The human HCC cell line HuH7 (20) and the mouse HCC cell line BNL 1ME A.7R.1 (BNL) were cultured in DMEM (Invitrogen Life Technologies)

supplemented with 10% heat-inactivated FBS (Invitrogen Life Technologies). When infected with Ad-tk-MCP1 or Ad-MCP1, BNL cells produced MCP-1 protein at similar levels as HuH7 cells (data not shown), suggesting that human MCP-1 protein was efficiently expressed in the infected human and mouse HCC cell lines.

Preparation of dendritic cells (DCs) and monocytes

Murine DCs were generated using the method of Lutz et al. (21). Briefly, bone marrow cells were harvested from 6-wk-old male BALB/c-*nu/nu* mice (CLEA Japan). Erythrocytes were lysed with ammonium chloride potassium buffer (BioWhittaker), and the nucleated cells were plated in plastic bacteriologic dishes in 10 ml of RPMI 1640 supplemented with 10% heat-inactivated FBS and 20 ng/ml murine GM-CSF (PeproTec), with the culture medium refreshed every 3 days. On day 8, the nonadherent DCs were collected. Purity was routinely >95% $CD11c^+$ DC as determined by FACS analysis.

Thioglycollate-elicited murine peritoneal exudate cells were collected as described (22). Briefly, nude mice were i.p. injected with 2 ml of 3% fluid thioglycollate medium (Wako Pure Chemical) and sacrificed 4 days later, followed by peritoneal lavage with 10 ml of cold PBS. Approximately 90% of the collected peritoneal cells were positive for both Mac-1 (CD11b) and $I\text{-}A^d$ MHC class II when stained with PE-conjugated anti-Mac-1 Ab (clone M1/70; BD Pharmingen) and FITC-conjugated $I\text{-}A^d$ MHC class II (clone AMS-32.1; BD Pharmingen).

Human monocytes and DCs were isolated from healthy blood donors (23). Briefly, PBMCs were isolated by centrifugation in Lymphoprep tubes (Nycomed). PBLs were then incubated in 6-well cell culture plates and the resultant adherent cells were collected as a monocyte population consisting of ~70% $CD14^+$ (clone MφP9; BD Pharmingen) cells, as determined by flow cytometric analysis. The monocyte population was further grown into differentiated DCs by culturing them for 1 wk in CellGro DC medium (Good Manufacturing Practice grade; Cell Genix) supplemented with 100 ng/ml GM-CSF (Cell Genix) and 50 ng/ml IL-4 (Cell Genix). The cells were collected with viability of >80%, and >60% of cells were identified as $CD14^-HLA\text{-}DR^+$ (clone L243; BD Pharmingen) DCs.

Assays for IL-12 production in vitro

HuH7 cells were infected with Ad-tk-MCP1, Ad-tk, or Ad-lacZ at a multiplicity of infection (MOI) of 5 for 24 h. Aliquots of 10^5 DCs or monocytes were cocultured with 10^5 rAd- or mitomycin C (MMC)-treated HuH7 cells in 1.0 ml of culture medium in a 24-well tissue culture plate and treated with or without GCV for two days at 37°C. The concentrations of IL-12 in the medium were quantitated using an immunoassay kit (BioSource International).

Animal studies

The following investigations were conducted in accordance with the Institutional Animal Care and Use Committee guidelines of Kanazawa University. Six-week-old male athymic nude mice were s.c. injected with 5×10^6 HuH7 cells on day 0. On days 3 and 4, 5×10^7 $TCID_{50}$ (100 μl) of Ad-tk-MCP1, Ad-tk, or Ad-MCP1 was injected into the s.c. tumors, and the mice were treated with 75 mg/kg GCV injected into the peritoneal cavity every day for the next 5 days (days 5–9). Following complete eradication of the primary tumors, the mice were s.c. rechallenged on day 14 with 3×10^6 HuH7 cells or injected with 1×10^3 BNL cells at a distance of >3 cm from the primary challenge site. Nine of 80 (11.3%) mice treated with Ad-tk-MCP1 and 9 of 44 (20.4%) treated with Ad-tk did not show a complete eradication of the primary tumor by the final measurement and therefore were excluded from a rechallenge experiment. In some experiments, Ad-tk-MCP1-treated animals were i.p. administered 200 μl of 1 mg/ml polyclonal rabbit anti-asialo GM1 (AGM1) Ab (Wako Pure Chemical), an Ab against NK cells (24, 25), or 200 μl of rabbit serum (Sigma-Aldrich), 1 ml of 2 mg/ml carrageenan (Sigma-Aldrich), which inactivates macrophages in vivo (26–28), or 1 ml of PBS on days 11, 12, 13, 20, 27, 34, 41, and 48. In another series of experiments, Ad-tk-MCP1-treated animals were i.p. administered 250 μg of neutralizing goat anti-mouse IL-12 Ab (Sigma-Aldrich), 225 μg of anti-IL-12 Ab plus 25 μg of anti-mouse IL-18 Ab (93-10C; Medical & Biological Laboratories), or 250 μg of control IgG Ab (goat and/or rat; Sigma-Aldrich) on days 14 and 17. Tumor sizes were measured every 4 days after the second tumor injection, and tumor volumes were calculated according to the formula (longest diameter) × (shortest diameter)²/2.

In another series of experiments, immunocompetent BALB/c-jcl mice (CLEA Japan) were s.c. injected with 1×10^5 BNL cells infected with each rAd at an in vitro MOI of 100 on day 0, GCV was administered i.p. for the next 5 days (days 1–5), and the primary tumors were completely eradicated. These mice were s.c. injected with 1×10^4 BNL cells in other sites on day 14, and the tumor sizes were measured every 7 days.

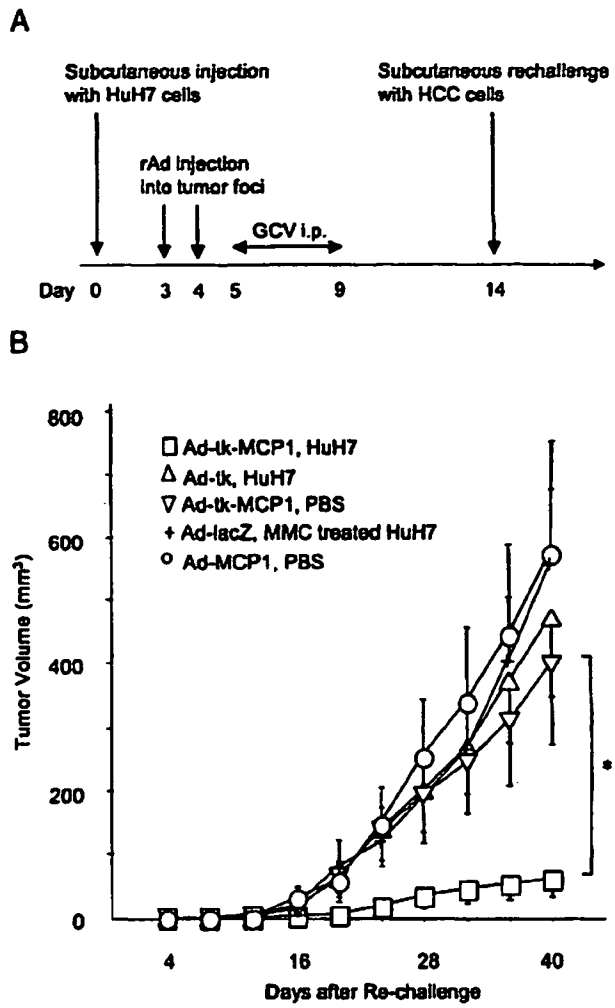

FIGURE 2. Prolonged antitumor effects of rAds expressing HSV-tk with or without MCP-1 in an athymic nude mouse model of HCC. *A*, Mice were s.c. injected with 5×10^6 HuH7 cells on day 0. On days 3 and 4, 5×10^7 $TCID_{50}$ of Ad-tk-MCP1, Ad-tk, Ad-lacZ, or Ad-MCP1 were injected into the tumors, and the mice were i.p. injected with 75 mg/kg GCV every day for the next 5 days (days 5–9). Following complete eradication of the primary tumors, the mice were s.c. rechallenged with 3×10^6 HuH7 cells at other sites on day 14. *B*, Tumor sizes were measured every 4 days. The results are the means of three independent experiments. *, $p < 0.001$ compared to Ad-tk with HuH7 (Ad-tk, HuH7) by the Mann-Whitney's *U* test.

ELISA for serum IL-12 and IL-18

Mouse sera were collected before the injection of s.c. primary tumors and after the rechallenge with tumors, and IL-12 and IL-18 concentrations were measured using immunoassay kits (IL-12 from BioSource International and IL-18 from Medical & Biological Laboratories).

Immunohistochemical analysis

Tumor tissues and spleens were resected on day 16 (2 days after tumor rechallenge). The tissue samples, except those used for F4/80 (A3-1; Serotec) staining, were embedded in OCT compound (Sakura Finetek) and snap frozen in liquid nitrogen. Cryostat sections of frozen tissues were fixed in cold acetone for 10 min, followed by rinsing three times in PBS. The tissue samples used for F4/80 staining were fixed *in 10% phosphate*-buffered formalin and embedded in paraffin. To avoid nonspecific staining,

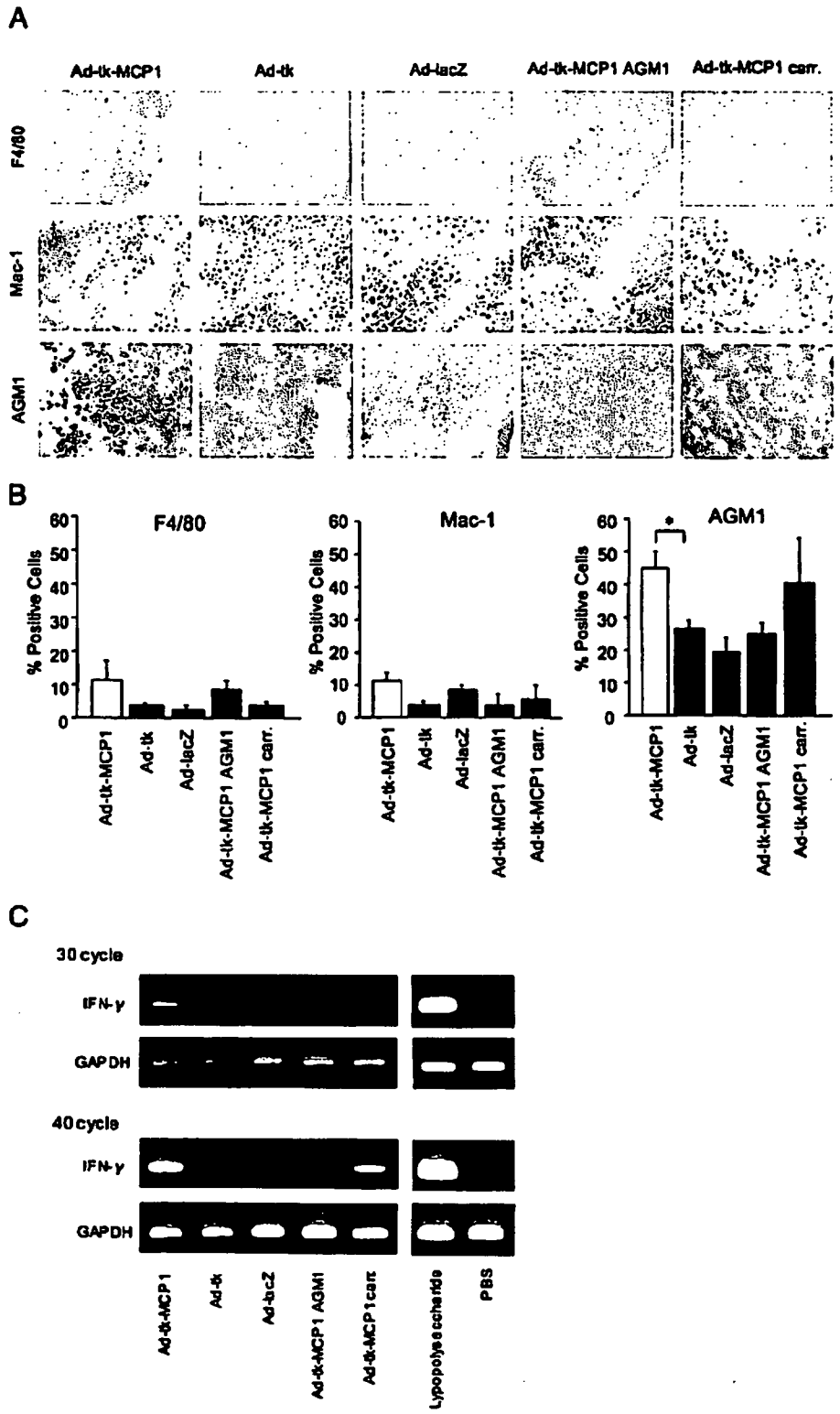

FIGURE 3. Expression of AGM1, F4/80, and Mac-1 Ags and IFN-γ mRNA in rechallenged tumor tissues. In the experiment described in the legend to Fig. 2, tumor tissues were resected 2 days after tumor rechallenge and analyzed immunohistochemically and estimated for IFN-γ mRNA expression by RT-PCR. *A*, Tumor tissues obtained from mice whose primary tumors were treated with Ad-tk-MCP1, Ad-tk, and Ad-LacZ were stained with anti-AGM1, F4/80, and Mac-1 Abs. Original magnification, ×100. *B*, Quantitative morphometric analysis showing the proportions of positive cells in areas of 100 tumor cells. Values are the means ± SE of triplicate experiments. *, $p < 0.05$ compared to Ad-tk by the Mann-Whitney's *U* test. *C*, RT-PCR were conducted in accordance with the manufacture's protocol as described in *Materials and Methods*. Bands corresponding to IFN-γ (384 bp) and GAPDH (265 bp) were detected. Splenocytes treated with 1 μg/ml LPS were used as a positive marker and tumor tissues treated with PBS were used as a negative control. carr., Carrageenan.

avidin and biotin in the tissues were blocked using a blocking kit (Vector Laboratories). The slides were subsequently incubated with Abs against AGM1, F4/80, Mac-1, CD11c (HL3; BD Pharmingen), or CD45R (RA3-6B2; BD Pharmingen) for 30 min at room temperature. Negative controls included staining with the corresponding isotype for each Ab and subsequent staining with the secondary Ab. The reactions were visualized using a VECTASTAIN ABC Standard kit (Vector Laboratories), followed by counterstaining with hematoxylin.

RT-PCR for IFN-γ gene expression

Total RNA was extracted from tumor tissues resected on day 10 using a total cellular RNA isolation kit (Ambion) according to the manufacturer's protocol. Each RT-PCR was performed using 1 μg of total RNA and an oligo(dT) adaptor primer and an RNA PCR kit (avian myeloblastosis virus), version.2.1 (Takara Bio). The amplification protocol consisted of an initial denaturation at 94°C for 2 min followed by 30 or 40 cycles of

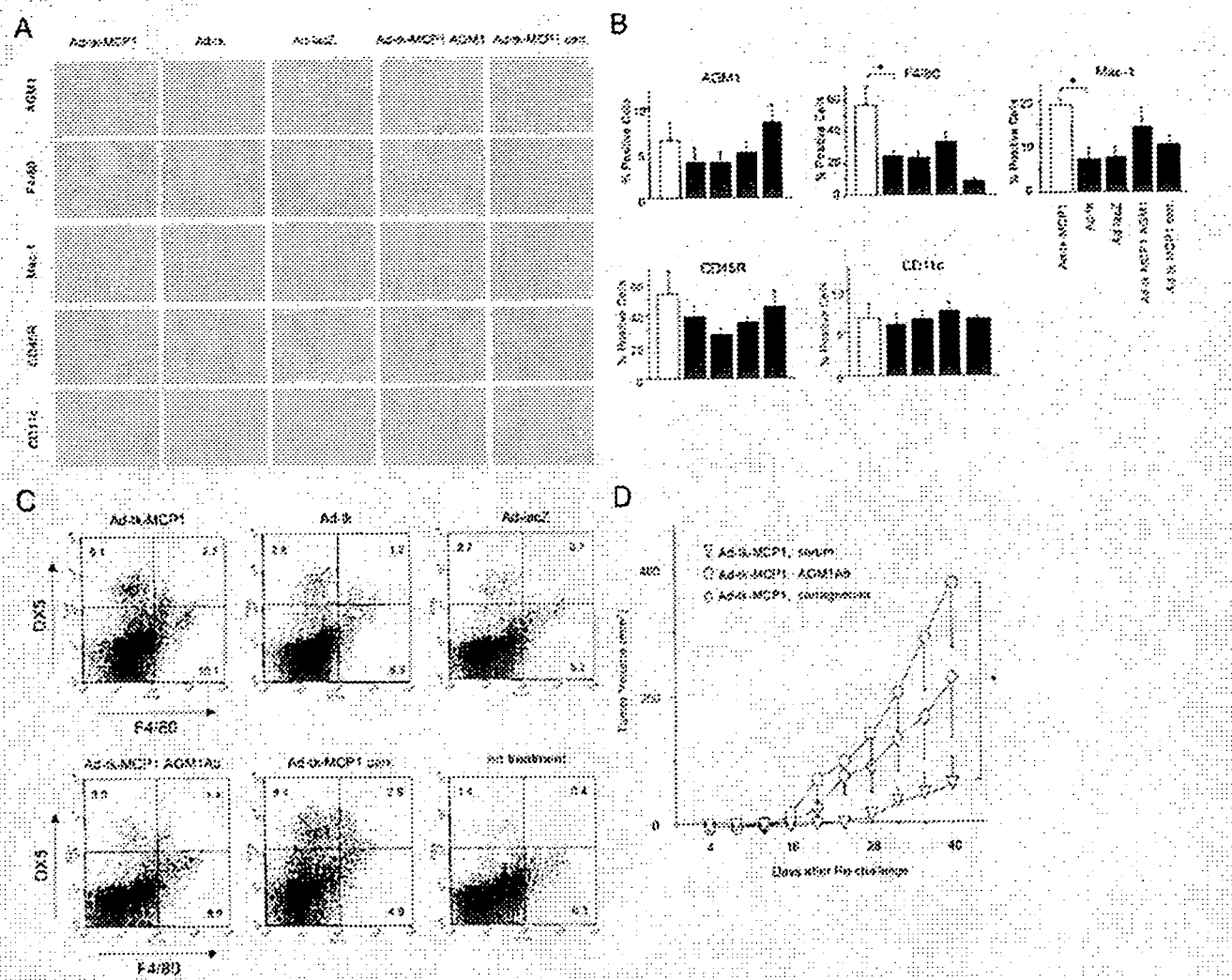

FIGURE 4. *A–C*, Immunohistochemical detection of AGM1, F4/80, Mac-1, CD11c, and CD45R in spleens. In the experiment described in the legend to *Fig. 3*, spleens were resected 2 days after the tumor rechallenge. *A*, The numbers of immune cells in the spleens were analyzed immunohistochemically using Abs against AGM1, F4/80, Mac-1, CD11c, and CD45R. Original magnification, ×100. *B*, Quantitative morphometric analysis showing the percentage of positive cells in 30 × 400 power fields. Each value is the mean ± SE of triplicate experiments. *, $p < 0.05$ compared with Ad-tk by the Mann-Whitney *U* test. *C*, Surface expression of DX5 and F4/80 in cell populations obtained from spleens was assessed by FACS. The results are representative of two independent experiments. carr., Carrageenan. *D*, The effects of anti-AGM1 Ab or carrageenan on the growth of rechallenged tumors. At the rechallenge with HuH7 cells, Ad-tk-MCP1-treated animals were i.p. administered with 200 μl of 1 mg/ml anti-AGM1 Ab (Ad-tk-MCP1, AGM1 Ab), 200 μl of rabbit serum (Ad-tk-MCP1, serum) or 1 ml of 2 mg/ml carrageenan (Ad-tk-MCP1, carrageenan) as described in *Materials and Methods*. Tumor sizes were measured every 4 days. The results are the means of two independent experiments. *, $p < 0.05$ compared to Ad-tk-MCP1 with PBS or serum (Ad-tk-MCP1, serum) by the Mann-Whitney *U* test.

denaturation at 94°C for 30 s, annealing at 60°C for 30 s, and an extension at 72°C for 1.5 min. The PCR primers for the mouse IFN-γ and GAPDH genes were purchased from R&D Systems.

Flow cytometry

Single cell suspensions of splenocytes were resuspended in PBS containing 1% BSA and 0.1% sodium azide and incubated for 30 min on ice with FITC-conjugated rat anti-mouse F4/80 and PE-conjugated rat anti-mouse pan NK cells (DX5; BD Pharmingen) or with FITC-conjugated rat anti-mouse CD4 (BD Pharmingen) and PE-conjugated rat anti-mouse CD8 (BD Pharmingen). The cells were washed, resuspended in PBS, and analyzed in a FACScan with CellQuest software.

Statistical analysis

All results were expressed as means ± SE. The statistical significance of differences between groups was evaluated by repeated measures ANOVA for the duration of the serum levels of IL-12 or the Mann-Whitney *U* test for the other results.

Results

Apoptotic HCC cells expressing MCP-1 augment IL-12 production by monocytes and DCs in vitro

IL-12, which was originally identified as an NK-stimulatory factor and a cytotoxic lymphocyte maturation factor, is one of the most promising cytokines in cancer treatment because of its multiple effects. IL-12 is produced by APCs such as macrophages, DCs, and B cells following the appropriate stimuli (29–31). To evaluate the immunomodulatory effects of rAds expressing HSV-tk with or without MCP-1 (Fig. 1), we measured IL-12 production by monocytes and DCs, both of which had been cocultured with HCC cells that had been infected with rAds (Fig. 1). Murine peritoneal exudate cells, consisting mostly of macrophages, and human monocytes cocultured with apoptotic HCC cells induced by the HSV-tk/GCV system plus MCP-1 produced greater amounts of IL-12

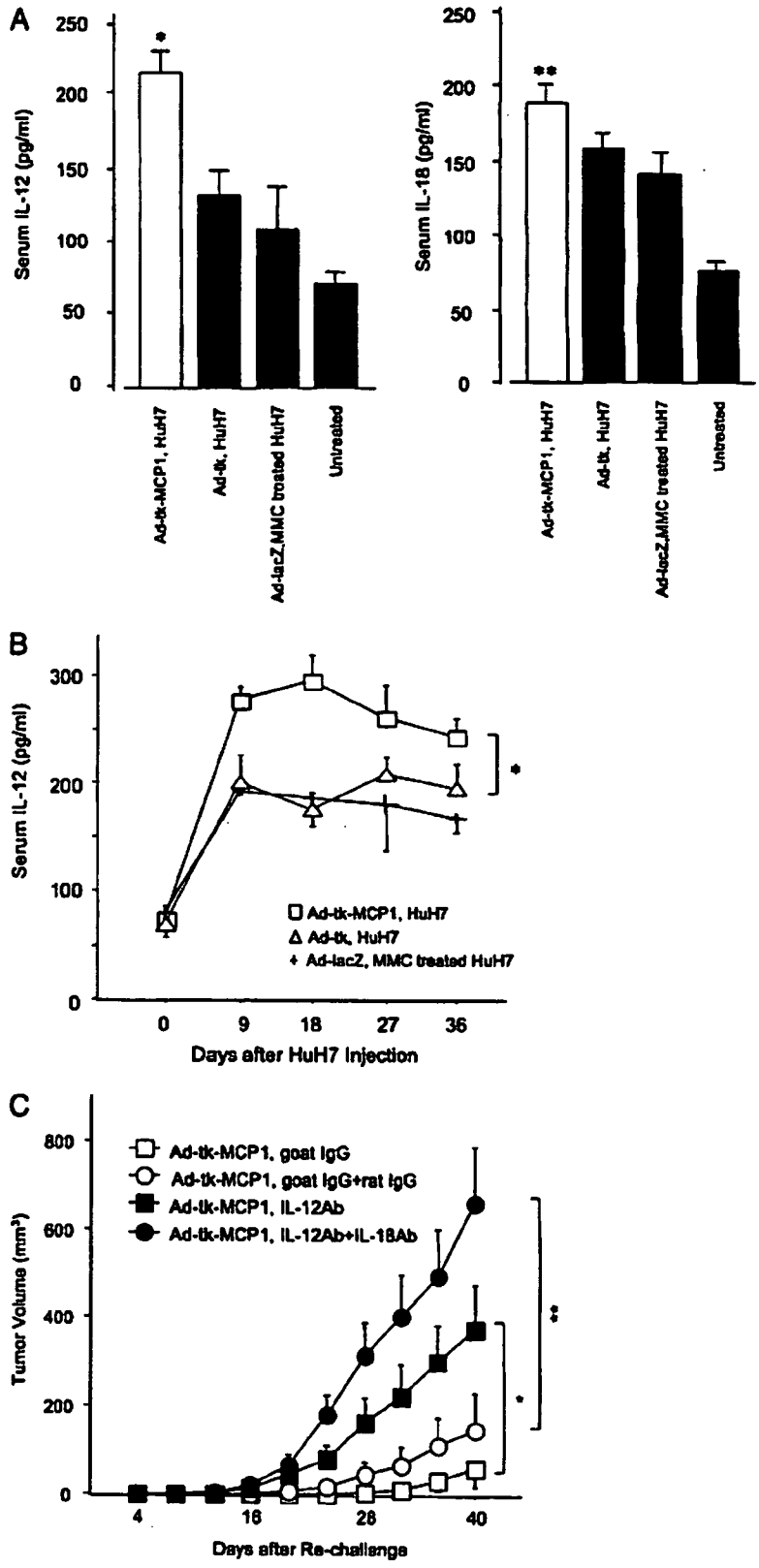

FIGURE 5. Roles of IL-12 and IL-18 in growth suppression of rechallenged HuH7 cells. *A*, Mouse sera were collected before s.c. injection of primary tumor cells (untreated) and 2 days after rechallenge with HuH7 cells, and IL-12 and IL-18 concentrations were measured using immunoassay kits. Each value is the mean ± SE of triplicate experiments. *, $p < 0.01$; **, $p < 0.05$ compared to Ad-tk by the Mann-Whitney *U* test. *B*, Serum concentrations of IL-12 were monitored every 9 days after the injection of primary tumors. Each value is the mean ± SE of triplicate experiments. *, $p < 0.05$ compared to Ad-tk with HuH7 (Ad-tk, HuH7) by repeated measures ANOVA. *C*, At rechallenge with HuH7 cells, Ad-tk-MCP1-treated animals were i.p. administered with 250 μg of anti-IL-12 Ab (Ad-tk-MCP1, IL-12Ab), 225 μg of anti-IL-12 Ab plus 25 μg of anti-IL-18 Ab (Ad-tk-MCP1, IL-12Ab+IL-18Ab), or 250 μg of control IgG Ab (Ad-tk-MCP1, goat IgG or Ad-tk MCP1, goat IgG+rat IgG). Tumor sizes were measured every 4 days. The results are representative of two independent experiments. *, $p < 0.05$ compared to Ad-tk-MCP1 with goat IgG (Ad-tk-MCP, goat IgG); **, $p < 0.01$ compared to Ad-tk-MCP1 with goat IgG plus rat IgG (Ad-tk-MCP, goat IgG+rat IgG) by the Mann-Whitney *U* test.

than did those cocultured with apoptotic HCC cells induced by the HSV-tk/GCV system alone (Fig. 1, *A* and *C*). Murine bone marrow DCs tended to produce IL-12 when cocultured with HCC cells infected with rAds expressing MCP-1 without regard to HSV-tk-induced apoptosis (Fig. 1*B*). Human DCs produced large amounts of IL-12 when cocultured with HSV-tk/GCV-induced apoptotic tumor cells, which expressed MCP-1, as did human monocytes (Fig. 1*D*). Thus, the phenomena observed in this xenograft model may also be observed under human allogeneic conditions.

When we measured DC maturation markers we found that their expression levels did not change when these cells were cocultured with tk/MCP-1 transduced HCC cells, whereas CD86 expression was elevated when the DCs were incubated with apoptotic HCC cells (data not shown).

Prolongation of the antitumor effects of the HSV-tk/GCV system by codelivery of the MCP-1 gene in an athymic nude mouse model of HCC

To determine the effects of HSV-tk/GCV plus MCP-1 in a murine model of HCC, HuH7 cells were s.c. transplanted into athymic nude mice and eradicated with rAds harboring HSV-tk with or without MCP-1, and the mice were rechallenged with HuH7 cells (Fig. 2*A*). We found that tumor regrowth was significantly lower when the primary tumor cells had been eradicated with Ad-tk-MCP1 as compared with Ad-tk (tumor volume 40 days after rechallenge, 59.2 ± 24.9 mm^3 (n = 22) vs 471.2 ± 118.6 mm^3 (n = 20), $p < 0.01$) (Fig. 2*B*). No growth inhibition was observed when Ad-tk-MCP1 or Ad-MCP1 was administered in the absence of HuH7 cell transplantation (tumor volume, 339.6 ± 124.3 mm^3, n = 18, and 575.3 ± 179.1 mm^3, n = 12, respectively) or when Ad-lacZ was administered along with MMC-treated HuH7 cells (tumor volume, 554.8 ± 125.6 mm^3, n = 18). The results demonstrate that, when the primary tumors were eradicated with the HSV-tk/GCV system plus MCP-1, the antitumor effects were maintained.

Recruitment and activation of NK cells in rechallenged tumors

Serum MCP-1 concentration was below the detection limit of the ELISA used when the s.c. tumors were injected with rAds, whereas the tumor produced MCP-1 in vitro upon infection with Ad-tk-MCP-1 (data not shown). Moreover, we could not detect adenovirus DNA in these rechallenged tumors by using PCR (data not shown), negating the possibility that adenovirus infection contributed to the rejection of the rechallenged tumor. These results indicate that the injected human MCP-1 gene functioned locally in the primary s.c. tumors, thereby modulating the subsequent response to the rechallenged tumor. Because athymic nude mice possess NK cells and macrophages but not T lymphocytes, we determined the migration of these cells by an immunohistochemical analysis. The number of $AGM1^+$ NK cells was significantly higher upon tumor rechallenge in mice whose primary tumors had been eradicated with Ad-tk-MCP1 plus GCV than in those whose primary tumors had been eradicated with Ad-tk plus GCV ($p < 0.05$) (Fig. 3, *A* and *B*). Similarly, the numbers of F4/80 or Mac-1 positive cells (32, 33) tended to be higher upon tumor rechallenge in mice whose primary tumors had been eradicated with Ad-tk-MCP1. Moreover, the mRNA of IFN-γ secreted by NK cells (34) became detectable after 30 PCR cycles in the rechallenged tumors of animals whose primary tumors had been eradicated with Ad-tk-MCP1 and was greatly amplified after 40 PCR cycles (Fig. 3*C*). These results demonstrate that NK cells were recruited and activated into rechallenged tumor tissues, presumably inhibiting tumor cell growth in mice whose primary tumors had been eradicated with HSV-tk/GCV plus MCP-1.

To monitor the activation state of innate immunity in extrahepatic lymphoid organs, we determined immunohistochemically the numbers of immune cells in the spleen after tumor rechallenge using anti-AGM1, F4/80, Mac-1, CD11c, and CD45R Abs (Fig. 4, *A* and *B*). The numbers of $F4/80^+$ and $Mac\text{-}1^+$ cells were significantly increased in the spleens of mice treated with Ad-tk-MCP1 compared with mice treated with Ad-tk ($p < 0.05$). In contrast, the numbers of $AGM1^+$ and $CD45R^+$ cells tended to be higher in the spleens of mice treated with Ad-tk-MCP1, but there was little difference in the numbers of $CD11c^+$ cells. A flow cytometrical analysis of splenocyte single cell suspensions demonstrated that the numbers of $DX5^+$ and $F4/80^+$ cells tended to be higher in the spleens of mice treated with Ad-tk-MCP1 (Fig. 4*C*). In contrast, treatment with carrageenan decreased the number of macrophages in the spleen and at rechallenge sites and slightly increased the number of NK cells in the spleen. Collectively, these results suggest that alterations in the proportions of cell subsets in splenocytes may reflect the activation status of the innate immune system following the eradication of primary tumors by HSV-tk/GCV plus MCP-1. Finally, an anti-AGM1 Ab (35, 36) significantly inhibited the antitumor immunity conferred by Ad-tk-MCP1 (tumor volume 40 days after rechallenge, 385.4 ± 106.3 mm^3 (n = 22) vs 64.2 ± 43.6 mm^3 (n = 16), $p < 0.05$), and carrageenan partially inhibited the antitumor immunity of Ad-tk-MCP1 (tumor volume, 242.6 ± 100.8 mm^3 (n = 14) vs 53.8 ± 22.9 mm^3 (n = 22), p = 0.22) (Fig. 4*D*). The results indicate that antitumor effects were mainly mediated by NK cells.

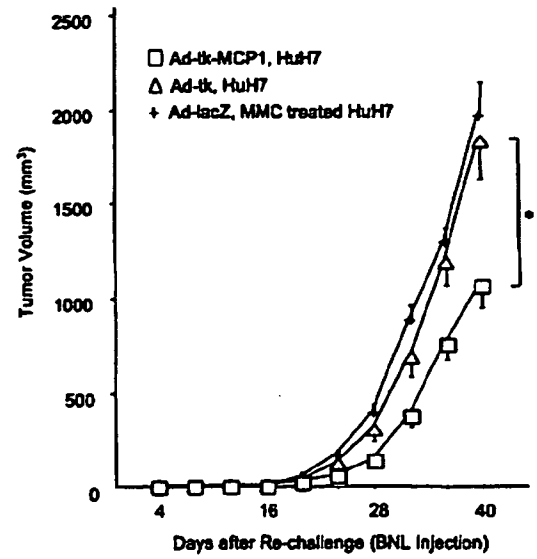

FIGURE 6. Antitumor effects of rAds expressing HSV-tk with or without MCP-1 against a second unprimed cell line (BNL) in an athymic nude mouse model of HCC. As described in the legend to Fig. 3, following complete eradication of the primary tumors the mice were s.c. injected with 1×10^3 BNL cells at other sites on day 14. Tumor sizes were measured every four days. The results are the means of two independent experiments. •, $p < 0.01$ compared to Ad-tk with HuH7 (Ad-tk, HuH7) by the Mann-Whitney's U test.

Involvement of IL-12 and IL-18 in sustained antitumor effects

IL-18 is a proinflammatory cytokine produced by activated macrophages that has been shown to augment both innate and acquired immunity (37) and, in combination with IL-12, induce Th 1 cell development and NK cell activation (38). We therefore assayed IL-12 and IL-18 production after tumor rechallenge. Serum concentrations of IL-12 and IL-18 were significantly higher after tumor rechallenge in mice whose primary tumors had been eradicated with Ad-tk-MCP1 compared with mice whose tumors had been eradicated with Ad-tk ($p < 0.05$) (Fig. 5*A*). Moreover, serum concentrations of IL-12 peaked after primary tumors were eradicated (day 9) and were sustained thereafter ($p < 0.05$) (Fig. 5*B*). Furthermore, the administration of anti-IL-12 significantly inhibited the antitumor effects conferred by Ad-tk-MCP1 (Fig. 5*C*) and reduced the serum concentrations of IL-12 to an undetectable level

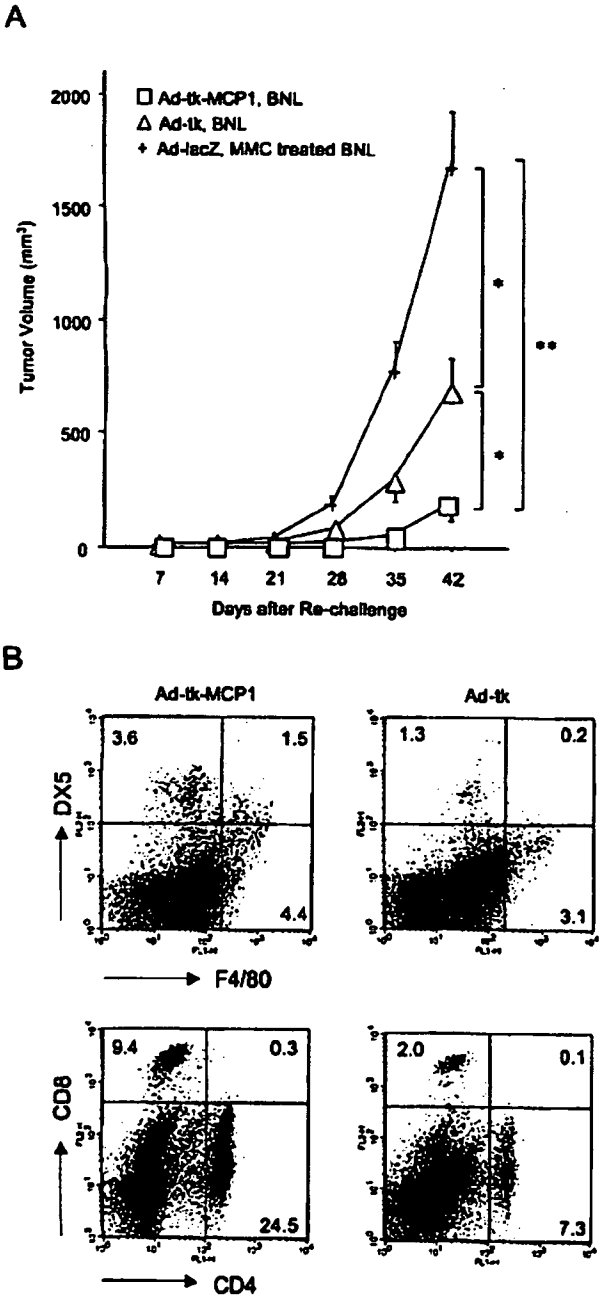

FIGURE 7. Prolonged antitumor effects of rAds expressing HSV-tk with or without MCP-1 in an immunocompetent mouse model of HCC. *A*, On day 0, mice were s.c. injected with 1×10^5 BNL cells infected with Ad-tk-MCP1, Ad-tk, or Ad-lacZ at an in vitro MOI of 100. The mice were i.p. injected with 75 mg/kg GCV per day for the next 5 days (days 1–5). Following complete eradication of the primary tumors, the mice were s.c. rechallenged with 1×10^4 BNL cells at other sites on day 14. Tumor sizes were measured every 7 days. The results are the means of three independent experiments. **, $p < 0.001$ compared to Ad-lacZ with MMC-treated BNL (Ad-lacZ, MMC treated BNL); *, $p < 0.01$ compared to Ad-tk with BNL (Ad-tk, BNL) or Ad-lacZ with MMC-treated BNL (Ad-lacZ, MMC-treated BNL) by the Mann-Whitney *U* test. *B*, Spleens were resected 70 days after the injection of primary tumor cells, and surface expression of DX5, F4/80, CD4, and CD8 in cell populations obtained from spleens was assessed by FACS. The results are representative of two independent experiments.

(data not shown). The combined treatment of anti-IL-12 and anti-IL-18 Ab further diminished antitumor effects (Fig. 5*C*) and reduced both serum IL-12 and IL-18 levels to undetectable levels (data not shown). The results suggest the critical involvement of IL-12 and IL-18 in the antitumor effects induced by Ad-tk-MCP1 on tumor regrowth.

Innate immune responses to heterologous tumor injection in an athymic nude mouse

To estimate the involvement of innate immune responses in the antitumor effects observed with HSV-tk/GCV plus MCP-1, we rechallenged mice with heterologous tumor administration. The growth of a second unprimed cell line (BNL; transformed liver cells derived from BALB/c mice) was significantly suppressed when HuH7 cells had been eradicated with Ad-tk-MCP1 as compared with Ad-tk (tumor volume, 1059.5 ± 110.6 mm^3 ($n = 12$) vs 1825.4 ± 197.9 mm^3 ($n = 12$), $p < 0.01$) when Ad-lacZ was administered with MMC-treated HuH7 cells (tumor volume, 1960.8 ± 183.8 mm^3, $n = 12$) (Fig. 6). These results indicate that the innate immune responses contributed to the prolonged antitumor effects of HSV-tk/GCV plus MCP-1 gene transfer.

Prolonged antitumor effects against mouse HCC of rAd expressing HSV-tk and MCP-1 in an immunocompetent mouse

Finally, we evaluated the antitumor responses in immune-competent mice using the same experimental procedures (Fig. 7*A*). The growth of rechallenged tumors was significantly lower when the primary tumor cells had been eradicated with Ad-tk-MCP1 as compared with Ad-tk (tumor volume 42 days after rechallenge, 170.3 ± 54.2 mm^3 ($n = 22$) vs 488.9 ± 120.1 mm^3 ($n = 22$), $p < 0.01$), similarly observed on athymic nude mice injected with human HCC. In addition, the growth of rechallenged tumors was significantly suppressed in mice whose primary tumors had been eradicated with Ad-tk as compared with those treated with Ad-lacZ and MMC (488.9 ± 120.1 mm^3 ($n = 22$) vs 1666.4 ± 259.2 mm^3 ($n = 22$), $p < 0.01$). Furthermore, when we isolated splenocytes 70 days after the injection of primary tumor cells we found that the numbers of $CD4^-$ and $CD8^+$ cells were increased in mice treated with Ad-tk-MCP1 (Fig. 7*B*). Collectively, these results confirm that antitumor effects may be dependent not only on innate immunity but on acquired immune responses.

Discussion

In the current study, we observed that when monocytes were cocultured with apoptotic HCC cells infected with Ad-tk-MCP1, these immune cells produced large amounts of IL-12. Interestingly, in both nude and immunocompetent mice the growth of rechallenged HCC cells was markedly suppressed after the primary tumor cells had been eradicated with Ad-tk-MCP1 followed by GCV administration. Furthermore, these prolonged in vivo antitumor effects were associated with the production of IL-12 and IL-18 and mediated by NK cells.

Monocytes produced large amounts of IL-12 when cocultured with apoptotic HCC cells induced by the HSV-tk/GCV system plus MCP-1. APCs, such as macrophages, DCs, and B cells produce IL-12, which was originally identified as an NK-stimulatory factor and shown to exhibit considerable antineoplastic activity (39, 40). APCs were found to be activated upon the recognition of Ags from apoptotic target cells (41), and both macrophages and DCs secrete large amounts of IL-12 when treated with MCP-1 in vitro (33, 42, 43). These findings suggest that the recognition of apoptotic tumor cells together with MCP-1 may activate macrophages and DCs, thereby enhancing IL-12 secretion.

We demonstrated that the antitumor effects were maintained when the tumor cells had been eradicated with Ad-tk-MCP1, a vector that expresses both a suicide gene and a chemokine, but that either alone was not sufficient to prolong immunity in our models.

We previously demonstrated that MCP-1 secreted by apoptotic HuH7 cells may recruit and activate macrophages efficiently, although these effects did not occur when the tumor cells were treated with the rAd expressing either HSV-tk or MCP-1 (8, 10). Moreover, we observed that the numbers of Mac-1$^+$ and F4/80$^+$ cells were increased in the spleens of mice after tumor rechallenge. Indeed, MCP-1 has been shown to activate murine peritoneal macrophages and enhance the expression of CD11b (Mac-1) in BALB/c mice (32, 33). Collectively, these results suggest that during eradication of the primary tumors, activated macrophages in the tumor tissues and the peripheral lymphoid organs can induce the secretion of cytokines, including IL-12 and IL-18, that can activate NK cells, thus exerting antitumor effects.

IL-12-stimulated NK cells exhibit potent cytotoxic activity against various tumor cells (31, 44, 45). NK cells are a part of the innate immune system, a first-line defense against tumor cells, and exert antitumor effects of NK cells rapidly without any prior sensitization (46). The depletion of NK cells has been shown to promote metastases or tumor growth after rechallenge with primary tumor cells (15, 44, 47). We demonstrated here that the growth of rechallenged parental tumor cells or newly challenged heterologous tumor cells was suppressed after eradication of the primary tumors. Therefore, augmentation of NK-mediated innate immune responses may be an attractive strategy for preventing HCC recurrence, including the growth of differentially transformed tumor cells.

We observed that NK cell-mediated antitumor effects were prolonged after primary tumor cells had been eradicated with Ad-tk-MCP1. Several lines of evidence indicate that the inhibitory effects of NK cells on tumor growth were maintained and were detectable at the site of the primary tumor even after treatment discontinuation (36, 48). Although the mechanisms involved in these responses are not yet known, a number of tumor model systems have demonstrated the important roles of NK cells in early tumor clearance, leading to the establishment of adaptive immunity. It was recently reported that NK cell-mediated immune responses featured hallmarks of adaptive immunity such as acquired immunity, long-lived memory, and Ag specificity (16). DCs expressing IL-12 have been shown to confer NK-mediated tumor protection in which NK activation is dependent on both DC-NK interaction and IL-12 secretion (49). Moreover, NK cell-derived IFN-γ may provide early immune regulation that alters the outcome and quality of adaptive immunity (50). Furthermore, MCP-1 has been shown to induce DC migration to lesions where NK cytolytic responses are activated (51). Consistent with these observations, we demonstrated that the antitumor responses were abolished when NK cells were inactivated by treatment with the AGM1 Ab and that NK cells were recruited and IFN-γ production enhanced in the rechallenged tumors.

We observed that the growth of rechallenged heterologous tumors was suppressed to a lesser extent than that of homologous tumors in our nude mice model. Athymic nude mice lack T lymphocyte-mediated immune responses, but the numbers and functions of macrophages and NK cells are preserved. Moreover, nude mice have limited populations of extrathymically matured T lymphocytes, including $\gamma\delta$ T cells (52), and these may be reduced slightly by treatment with AGM1 Ab (53). Both NK cells and Vδ1γ δT lymphocytes have been reported to prevent the growth of s.c. melanoma cells, with both cell types detected at the sites of the s.c. tumors (47). Therefore, we cannot exclude the possibility that the memory subset of γ δT cells affects antitumor immunity against homologous and heterologous cells, thus leading to differences in the magnitude of tumor suppression.

Although the results presented here are promising, a number of problems remain to be solved before this approach can be used clinically. First, s.c. tumor models using an HCC cell line may not be fully comparable to HCCs in patients. Second, problems using rAds need to be resolved before they can be applied clinically. However, in patients treated with nonsurgical procedures such as percutaneous radiofrequency ablation therapy and transcatheter arterial chemotherapy, the administration of rAd vectors may ensure tumor cell killing, thus enhancing the antitumor effects on residual tumor cells and recurrent HCC.

Acknowledgments

We thank Akemi Nakano and Yuzu Hasebe for assistance with histology and immunohistochemistry. We are also grateful to Maki Kawamura and Chiharu Minami for animal care.

Disclosures

The authors have no financial conflict of interest.

References

1. Venook, A. P. 1994. Treatment of hepatocellular carcinoma: too many options? *J. Clin. Oncol.* 12: 1323–1334.
2. Trinchet, J. C., and M. Beaugrand. 1997. Treatment of hepatocellular carcinoma in patients with cirrhosis. *J. Hepatol.* 27: 756–765.
3. Bruix, J. 1997. Treatment of hepatocellular carcinoma. *Hepatology* 25: 259–262.
4. Kuriyama, S., T. Sakamoto, K. Masui, T. Nakatani, K. Tominaga, M. Kikukawa, M. Yoshikawa, K. Ikenaka, H. Fukui, and T. Tsujii. 1997. Tissue-specific expression of HSV-tk gene can induce efficient antitumor effect and protective immunity to wild-type hepatocellular carcinoma. *Int. J. Cancer* 71: 470–475.
5. Kianmanesh, A. R., H. Perrin, Y. Panis, M. Fabre, H. J. Nagy, D. Houssin, and D. Klatzmann. 1997. A "distant" bystander effect of suicide gene therapy: regression of nontransduced tumors together with a distant transduced tumor. *Hum. Gene Ther.* 8: 1807–1814.
6. Okada, H., K. M. Giezeman-Smits, H. Tahara, J. Attanucci, W. K. Fellows, M. T. Lotze, W. H. Chambers, and M. E. Bozik. 1999. Effective cytokine gene therapy against an intracranial glioma using a retrovirally transduced IL-4 plus HSVtk tumor vaccine. *Gene Ther.* 6: 219–226.
7. Hall, S. J., S. E. Canfield, Y. Yan, W. Hassen, W. A. Selleck, and S. H. Chen. 2002. A novel bystander effect involving tumor cell-derived Fas and FasL interactions following Ad.HSV-tk and Ad.mIL-12 gene therapies in experimental prostate cancer. *Gene Ther.* 9: 511–517.
8. Sakai, Y., S. Kaneko, Y. Nakamoto, T. Kagaya, N. Mukaida, and K. Kobayashi. 2001. Enhanced anti-tumor effects of herpes simplex virus thymidine kinase/ganciclovir system by codelivering monocyte chemoattractant protein-1 in hepatocellular carcinoma. *Cancer Gene Ther.* 8: 695–704.
9. Crittenden, M., M. Gough, K. Harrington, K. Olivier, J. Thompson, and R. G. Vile. 2003. Expression of inflammatory chemokines combined with local tumor destruction enhances tumor regression and long-term immunity. *Cancer Res.* 63: 5505–5512.
10. Tsuchiyama, T., S. Kaneko, Y. Nakamoto, Y. Sakai, M. Honda, N. Mukaida, and K. Kobayashi. 2003. Enhanced antitumor effects of a bicistronic adenovirus vector expressing both herpes simplex virus thymidine kinase and monocyte chemoattractant protein-1 against hepatocellular carcinoma. *Cancer Gene Ther.* 10: 260–269.
11. Allavena, P., G. Bianchi, D. Zhou, J. van Damme, P. Jilek, S. Sozzani, and A. Mantovani. 1994. Induction of natural killer cell migration by monocyte chemotactic protein-1, -2 and -3. *Eur. J. Immunol.* 24: 3233–3236.
12. Maghazachi, A. A., A. al-Aoukaty, and T. J. Schall. 1994. C-C chemokines induce the chemotaxis of NK and IL-2-activated NK cells. Role for G proteins. *J. Immunol.* 153: 4969–4977.
13. Loetscher, P., M. Seitz, I. Clark-Lewis, M. Baggiolini, and B. Moser. 1996. Activation of NK cells by CC chemokines. Chemotaxis, Ca^{2+} mobilization, and enzyme release. *J. Immunol.* 156: 322–327.
14. Taub, D. D., T. J. Sayers, C. R. Carter, and J. R. Ortaldo. 1995. Alpha and beta chemokines induce NK cell migration and enhance NK-mediated cytolysis. *J. Immunol.* 155: 3877–3888.
15. Nokihara, H., H. Yanagawa, Y. Nishioka, S. Yano, N. Mukaida, K. Matsushima, and S. Sone. 2000. Natural killer cell-dependent suppression of systemic spread of human lung adenocarcinoma cells by monocyte chemoattractant protein-1 gene transfection in severe combined immunodeficient mice. *Cancer Res.* 60: 7002–7007.
16. O'Leary, J. G., M. Goodarzi, D. L. Drayton, and U. H. von Andrian. 2006. T cell- and B cell-independent adaptive immunity mediated by natural killer cells. *Nat. Immunol.* 7: 507–516.
17. Miyake, S., M. Makimura, Y. Kanegae, S. Harada, Y. Sato, K. Takamori, C. Tokuda, and I. Saito. 1996. Efficient generation of recombinant adenoviruses using adenovirus DNA-terminal protein complex and a cosmid bearing the full-length virus genome. *Proc. Natl. Acad. Sci. USA* 93: 1320–1324.

18. Sakai, Y., S. Kaneko, Y. Sato, Y. Kanegae, T. Tamaoki, I. Saito, and K. Kobayashi. 2001. Gene therapy for hepatocellular carcinoma using two recombinant adenovirus vectors with α-fetoprotein promoter and Cre/lox P system. *J. Virol. Methods* 92: 5–17.
19. Kanegae, Y., M. Makimura, and I. Saito. 1994. A simple and efficient method for purification of infectious recombinant adenovirus. *Jpn. J. Med. Sci. Biol.* 47: 157–166.
20. Nakabayashi, H., K. Taketa, T. Yamane, M. Miyazaki, K. Miyano, and J. Sato. 1984. Phenotypical stability of a human hepatoma cell line, HuH-7, in long-term culture with chemically defined medium. *Gann* 75: 151–158.
21. Lutz, M. B., N. Kukutsch, A. L. Ogilvie, S. Rossner, F. Koch, N. Romani, and G. Schuler. 1999. An advanced culture method for generating large quantities of highly pure dendritic cells from mouse bone marrow. *J. Immunol. Methods* 223: 77–92.
22. Kawaguchi, T., M. Suematsu, H. M. Koizumi, H. Mitsui, S. Suzuki, T. Matsuno, H. Ogawa, and K. Nomoto. 1983. Activation of macrophage function by intraperitoneal administration of the streptococcal antitumor agent OK-432. *Immunopharmacology* 6: 177–189.
23. Dhodapkar, M. V., R. M. Steinman, M. Sapp, H. Desai, C. Fossella, J. Krasovsky, S. M. Donahoe, P. R. Dunbar, V. Cerundolo, D. F. Nixon, and N. Bhardwaj. 1999. Rapid generation of broad T-cell immunity in humans after a single injection of mature dendritic cells. *J. Clin. Invest.* 104: 173–180.
24. Habu, S., H. Fukui, K. Shimamura, M. Kasai, Y. Nagai, K. Okumura, and N. Tamaoki. 1981. In vivo effects of anti-asialo GM1. I. Reduction of NK activity and enhancement of transplanted tumor growth in nude mice. *J. Immunol.* 127: 34–38.
25. Smyth, M. J., M. E. Wallace, S. L. Nutt, H. Yagita, D. I. Godfrey, and Y. Hayakawa. 2005. Sequential activation of NKT cells and NK cells provides effective innate immunotherapy of cancer. *J. Exp. Med.* 201: 1973–1985.
26. Ando, K., T. Moriyama, L. G. Guidotti, S. Wirth, R. D. Schreiber, H. J. Schlicht, S. N. Huang, and F. V. Chisari. 1993. Mechanisms of class I restricted immunopathology. A transgenic mouse model of fulminant hepatitis. *J. Exp. Med.* 178: 1541–1554.
27. Grosso, J. F., L. M. Herbert, J. L. Owen, and D. M. Lopez. 2004. MUC1/sec-expressing tumors are rejected in vivo by a T cell-dependent mechanism and secrete high levels of CCL2. *J. Immunol.* 173: 1721–1730.
28. Pulaski, B. A., M. J. Smyth, and S. Ostrand-Rosenberg. 2002. Interferon-γ-dependent phagocytic cells are a critical component of innate immunity against metastatic mammary carcinoma. *Cancer Res.* 62: 4406–4412.
29. Nanni, P., I. Rossi, C. De Giovanni, L. Landuzzi, G. Nicoletti, A. Stoppacciaro, M. Parenza, M. P. Colombo, and P. L. Lollini. 1998. Interleukin 12 gene therapy of MHC-negative murine melanoma metastases. *Cancer Res.* 58: 1225–1230.
30. Kodama, T., K. Takeda, O. Shimozato, Y. Hayakawa, M. Atsuta, K. Kobayashi, M. Ito, H. Yagita, and K. Okumura. 1999. Perforin-dependent NK cell cytotoxicity is sufficient for anti-metastatic effect of IL-12. *Eur. J. Immunol.* 29: 1390–1396.
31. Satoh, T., T. Saika, S. Ebara, N. Kusaka, T. L. Timme, G. Yang, J. Wang, V. Mouraviev, G. Cao, E. M. A. Fattah, and T. C. Thompson. 2003. Macrophages transduced with an adenoviral vector expressing interleukin 12 suppress tumor growth and metastasis in a preclinical metastatic prostate cancer model. *Cancer Res.* 63: 7853–7860.
32. Nesbit, M., H. Schaider, T. H. Miller, and M. Herlyn. 2001. Low-level monocyte chemoattractant protein-1 stimulation of monocytes leads to tumor formation in nontumorigenic melanoma cells. *J. Immunol.* 166: 6483–6490.
33. Biswas, S. K., and A. Sodhi. 2002. In vitro activation of murine peritoneal macrophages by monocyte chemoattractant protein-1: up-regulation of CD11b, production of proinflammatory cytokines, and the signal transduction pathway. *J. Interferon Cytokine Res.* 22: 527–538.
34. Carson, W. E., M. E. Ross, R. A. Baiocchi, M. J. Marien, N. Boiani, K. Grabstein, and M. A. Caligiuri. 1995. Endogenous production of interleukin 15 by activated human monocytes is critical for optimal production of interferon-γ by natural killer cells in vitro. *J. Clin. Invest.* 96: 2578–2582.
35. Nagai, M., and T. Masuzawa. 2001. Vaccination with MCP-1 cDNA transfectant on human malignant glioma in nude mice induces migration of monocytes and NK cells to the tumor. *Int. Immunopharmacol.* 1: 657–664.
36. van den Broeke, L. T., E. Daschbach, E. K. Thomas, G. Andringa, and J. A. Berzofsky. 2003. Dendritic cell-induced activation of adaptive and innate antitumor immunity. *J. Immunol.* 171: 5842–5852.
37. Okamura, H., S. Kashiwamura, H. Tsutsui, T. Yoshimoto, and K. Nakanishi. 1998. Regulation of interferon-γ production by IL-12 and IL-18. *Curr. Opin. Immunol.* 10: 259–264.
38. Dinarello, C. A., D. Novick, A. J. Puren, G. Fantuzzi, L. Shapiro, H. Muhl, D. Y. Yoon, L. L. Reznikov, S. H. Kim, and M. Rubinstein. 1998. Overview of interleukin-18: more than an interferon-γ inducing factor. *J. Leukocyte Biol.* 63: 658–664.
39. Brunda, M. J., L. Luistro, R. R. Warrier, R. B. Wright, B. R. Hubbard, M. Murphy, S. F. Wolf, and M. K. Gately. 1993. Antitumor and antimetastatic activity of interleukin 12 against murine tumors. *J. Exp. Med.* 178: 1223–1230.
40. Nastala, C. L., H. D. Edington, T. G. McKinney, H. Tahara, M. A. Nalesnik, M. J. Brunda, M. K. Gately, S. F. Wolf, R. D. Schreiber, W. J. Storkus, et al. 1994. Recombinant IL-12 administration induces tumor regression in association with IFN-γ production. *J. Immunol.* 153: 1697–1706.
41. Albert, M. L., B. Sauter, and N. Bhardwaj. 1998. Dendritic cells acquire antigen from apoptotic cells and induce class I-restricted CTLs. *Nature* 392: 86–89.
42. Matsukawa, A., C. M. Hogaboam, N. W. Lukacs, P. M. Lincoln, R. M. Strieter, and S. L. Kunkel. 2000. Endogenous MCP-1 influences systemic cytokine balance in a murine model of acute septic peritonitis. *Exp. Mol. Pathol.* 68: 77–84.
43. Traynor, T. R., A. C. Herring, M. E. Dorf, W. A. Kuziel, G. B. Toews, and G. B. Huffnagle. 2002. Differential roles of CC chemokine ligand 2/monocyte chemotactic protein-1 and CCR2 in the development of T1 immunity. *J. Immunol.* 168: 4659–4666.
44. Lasek, W., A. Mackiewicz, A. Czajka, T. Switaj, J. Golab, M. Wiznerowicz, G. Korczak-Kowalska, E. Z. Bakowiec-Iskra, K. Gryska, D. Izycki, and M. Jakobisiak. 2000. Antitumor effects of the combination therapy with TNF-α gene-modified tumor cells and interleukin 12 in a melanoma model in mice. *Cancer Gene Ther.* 7: 1581–1590.
45. Rakhmilevich, A. L., K. Janssen, Z. Hao, P. M. Sondel, and N. S. Yang. 2000. Interleukin-12 gene therapy of a weakly immunogenic mouse mammary carcinoma results in reduction of spontaneous lung metastases via a T-cell-independent mechanism. *Cancer Gene Ther.* 7: 826–838.
46. Kim, S., K. Iizuka, H. L. Aguila, I. L. Weissman, and W. M. Yokoyama. 2000. In vivo natural killer cell activities revealed by natural killer cell-deficient mice. *Proc. Natl. Acad. Sci. USA* 97: 2731–2736.
47. Orengo, A. M., E. Di Carlo, A. Comes, M. Fabbi, T. Piazza, M. Cilli, P. Musiani, and S. Ferrini. 2003. Tumor cells engineered with IL-12 and IL-15 genes induce protective antibody responses in nude mice. *J. Immunol.* 171: 569–575.
48. Lozupone, F., D. Pende, V. L. Burgio, C. Castelli, M. Spada, M. Venditti, F. Luciani, L. Lugini, C. Federici, C. Ramoni, et al. 2004. Effect of human natural killer and γδ T cells on the growth of human autologous melanoma xenografts in SCID mice. *Cancer Res.* 64: 378–385.
49. Miller, G., S. Lahrs, and R. P. Dematteo. 2003. Overexpression of interleukin-12 enables dendritic cells to activate NK cells and confer systemic antitumor immunity. *FASEB J.* 17: 728–730.
50. Ortaldo, J. R., and H. A. Young. 2003. Expression of IFN-γ upon triggering of activating Ly49D NK receptors in vitro and in vivo: costimulation with IL-12 or IL-18 overrides inhibitory receptors. *J. Immunol.* 170: 1763–1769.
51. Xu, L. L., M. K. Warren, W. L. Rose, W. Gong, and J. M. Wang. 1996. Human recombinant monocyte chemotactic protein and other C-C chemokines bind and induce directional migration of dendritic cells in vitro. *J. Leukocyte Biol.* 60: 365–371.
52. Dandekar, A. A., and S. Perlman. 2002. Virus-induced demyelination in nude mice is mediated by γ δ T cells. *Am. J. Pathol.* 161: 1255–1263.
53. Geldhof, A. B., J. A. Van Ginderachter, Y. Liu, W. Noel, G. Raes, and P. De Baetselier. 2002. Antagonistic effect of NK cells on alternatively activated monocytes: a contribution of NK cells to CTL generation. *Blood* 100: 4049–4058.

Available online at www.sciencedirect.com
ScienceDirect
Biochemical and Biophysical Research Communications 366 (2008) 186–192
BBRC
www.elsevier.com/locate/ybbrc

Comparative proteomic and transcriptomic profiling of the human hepatocellular carcinoma

Hirotaka Minagawa [a], Masao Honda [b,*], Kenji Miyazaki [c], Yo Tabuse [c,*], Reiji Teramoto [c], Taro Yamashita [b], Ryuhei Nishino [b], Hajime Takatori [b], Teruyuki Ueda [b], Ken'ichi Kamijo [a], Shuichi Kaneko [b]

[a] *Nano Electronics Research Laboratories, NEC Corporation, 34, Miyukigaoka, Tsukuba, Ibaraki 305-8501, Japan*
[b] *Department of Gastroenterology, Kanazawa University Graduate School of Medical Science, Kanazawa, 13-1 Takara-machi, Kanazawa 920-8641, Japan*
[c] *Bio-IT Center, NEC Corporation, 34, Miyukigaoka, Tsukuba, Ibaraki 305-8501, Japan*

Received 14 November 2007
Available online 4 December 2007

Abstract

Proteome analysis of human hepatocellular carcinoma (HCC) was done using two-dimensional difference gel electrophoresis. To gain an understanding of the molecular events accompanying HCC development, we compared the protein expression profiles of HCC and non-HCC tissue from 14 patients to the mRNA expression profiles of the same samples made from a cDNA microarray. A total of 125 proteins were identified, and the expression profiles of 93 proteins (149 spots) were compared to the mRNA expression profiles. The overall protein expression ratios correlated well with the mRNA ratios between HCC and non-HCC (Pearson's correlation coefficient: $r = 0.73$). Particularly, the HCC/non-HCC expression ratios of proteins involved in metabolic processes showed significant correlation to those of mRNA ($r = 0.9$). A considerable number of proteins were expressed as multiple spots. Among them, several proteins showed spot-to-spot differences in expression level and their expression ratios between HCC and non-HCC poorly correlated to mRNA ratios. Such multi-spotted proteins might arise as a consequence of post-translational modifications.

Keywords: Hepatocellular carcinoma; Proteome; Two-dimensional difference gel electrophoresis; Transcriptome; cDNA microarray

Hepatocellular carcinoma (HCC) is one of the most common cancers worldwide, and a leading cause of death in Africa and Asia [1]. Although several major risks related to HCC, such as hepatitis B and/or hepatitis C virus infection, aflatoxin B1 exposure, and alcohol consumption, and genetic defects, have been revealed [2], the molecular mechanisms leading to the initiation and progression of HCC are not well known. To find the molecular basis of hepatocarcinogenesis, comprehensive gene expression analyses have been done using many systems such as hepatoma cell lines and tissue samples [3,4]. Previously, we have carried out a comprehensive mRNA expression analysis using the serial analysis of gene expression (SAGE) [5] and cDNA microarray-based comparative genomic hybridization [6] to acquire the outline of gene expression profile of HCC. Although these genomic approaches have yielded global gene expression profiles in HCC and identified a number of candidate genes as biomarkers useful for cancer staging, prediction of prognosis, and treatment selection [7], the molecular events accompanying HCC development are not yet understood. In general, proteins rather than transcripts are the major effectors of cellular and tissue function [8] and it is accepted that protein expression do not always correlate with mRNA expression [9,10]. Thus, protein expression analysis, which could complement the available mRNA data, is also important to understand the molecular mechanisms of HCC.

* Corresponding authors. Fax: +81 76 234 4250 (M. Honda), +81 29 856 6136 (Y.Tabuse).
E-mail addresses: mhonda@medf.m.kanazawa-u.ac.jp (M. Honda), y-tabuse@cd.jp.nec.com (Y. Tabuse).

0006-291X/$ - see front matter © 2007 Elsevier Inc. All rights reserved.
doi:10.1016/j.bbrc.2007.11.101

The technique of two-dimensional difference gel electrophoresis (2D-DIGE), developed by Unlu et al. [11] is one of major advances in quantitative proteomics. Several groups have recently utilized 2D-DIGE to examine protein expression changes in HCC samples [12,13], whereas reports on the analysis combining both transcriptomic and proteomic approach are rare.

In the present study, we compared quantitatively protein expression profiles of HCC to non-HCC (non-cancerous liver) samples derived from 14 patients by 2D-DIGE. We also compared the protein expression profiles of the same HCC and non-HCC samples to the mRNA profiles which have been obtained using a cDNA microarray. The expression ratios of 93 proteins showed significant correlations with the mRNA ratios between HCC and non-HCC. Proteins involved in metabolic processes showed more prominent correlation. Our study describes an outline of gene and protein expression profiles in HCC, thus providing us a basis for better understanding of the disease.

Materials and methods

Patients. A total of 14 HCC patients who had surgical resection done in the Kanazawa University Hospital were enrolled. The clinicopathological characteristics of them are shown in Table 1. The HCC samples and adjacent non-tumor liver samples were snap frozen in liquid nitrogen, and used for cDNA microarray and 2D-DIGE analysis. All HCC and non-tumor samples were histologically diagnosed and quantitative detection of hepatitis C virus RNA by Amplicore analysis (Roche Diagnostic Systems) showed positive. The grading and staging of chronic hepatitis associated with non-tumor lesion were histologically assessed according to the method described by Desmet et al. [14] and histological typing of HCC was assessed according to Ishak et al. [15]. All strategies used for gene expression and protein expression analysis were approved by the Ethical Committee of Kanazawa University Hospital.

Preparation of cDNA microarray slides. In addition to in-house cDNA microarray slides consisting of 1080 cDNA clones as previously described [6,16–18], we made new cDNA microarray slides for detailed analysis of the signaling pathway of metabolism and enzyme function in liver disease [19]. Besides cDNA microarray analysis, a total of 256,550 tags were obtained from hepatic SAGE libraries (derived from normal liver, CH-C, CH-C related HCC, CH-B, and CH-B related HCC), including 52,149 unique tags. Among these, 16,916 tags expressing more than two hits were selected to avoid the effect of sequencing errors in the libraries. From these candidate genes, 9614 non-redundant clones were obtained from Incyte Genomics (Incyte Corporation), Clontech (Nippon Becton Dickinson), and Invitrogen (Invitrogen). Each clone was sequence validated and PCR amplified by Dragon Genomics (Takara Bio), and the cDNA microarray slides (Liver chip 10k) were constructed using SPBIO 2000 (Hitachi Software) as described previously [6,16–18].

Table 1
Characteristics of patients involved in this study

Patient No.	Age	Sex[a]	Histology of non-tumor lesion[b]	Tumor histology	Viral status
1	64	M	F4A1	Moderate	HCV
2	65	M	F4A1	Well	HCV
3	48	M	F3A1	Moderate	HCV
4	69	F	F4A2	Moderate	HCV
5	66	F	F4A2	Well	HCV
6	45	M	F4A1	Well	HCV
7	75	F	F4A1	Well	HCV
8	46	M	F4A2	Moderate	HCV
9	66	M	F2A2	Well	HCV
10	75	M	F3A1	Moderate	HCV
11	67	F	F4A2	Well	HCV
12	64	M	F4A1	Moderate	HCV
13	68	M	F4A0	Well	HCV
14	74	M	F1A0	Moderate	HCV

[a] M, male; F, female.
[b] F, fibrosis; A, activity.

RNA isolation and antisense RNA amplification. Total RNA was isolated from liver biopsy samples using an RNA extraction kit (Stratagene). Aliquots of total RNA (5 μg) were subjected to amplification with antisense RNA (aRNA) using a Message AmpTM aRNA kit (Ambion) as recommended by the manufacturer. About 25 μg of aRNA was amplified from 5 μg total RNA, assuming that 500-fold amplification of mRNA was obtained. The quality and degradation of the isolated RNA were estimated after electrophoresis using an Agilent 2001 bioanalyzer. In addition, 10 μg of aRNA was used for further labeling procedures.

Hybridization on cDNA microarray slides and image analysis. As a reference for each microarray analysis, aRNA samples prepared from the normal liver tissue from one of the patients were used. Test RNA samples fluorescently labeled with cyanine (Cy) 5 and reference RNA labeled with Cy3 were used for microarray hybridization as described previously [6,16–18]. Quantitative assessment of the signals on the slides was done by scanning on a ScanArray 5000 (General Scanning) followed by image analysis using GenePix Pro 4.1 (Axon Instruments) as described previously [6,16–18].

Protein expression analysis using 2D-DIGE. Protein samples were homogenized with lysis buffer (7 M urea, 2 M thiourea, 4% w/v CHAPS, 0.8 μM aprotinin, 15 μM pepstatin, 0.1 mM PMSF, 0.5 mM EDTA, 30 mM Tris–HCl, pH 8.5) and centrifuged at 13,000 rpm for 20 min at 4 °C. The supernatants were used as protein samples. The protein concentrations were determined with a protein assay reagent (Bio-Rad). The non-HCC and HCC samples (50 μg each) labeled with either Cy3 or Cy5 according to the manufacture's manual were combined and separated on 2-DE gels together with the Cy2-labeled internal standard (IS), which was prepared by mixing equal amounts of all samples. Analytical 2-DE was performed as described previously [20] using Immobiline DryStrip (pH 3–10, 24 cm, GE Healthcare) in the first dimension and 12.5% SDS–polyacrylamide gels (24 × 20 cm) in the second dimension. Samples were run in triplicate to obtain statistically reasonable results. After scanning with a Typhoon 9410 scanner (GE Healthcare), gels were silver stained for protein identification. For protein identification, 400 μg of the IS sample was also separately run on a 2-DE gel and stained with SYPRO Ruby (Invitrogen). All analytical and preparative gel images were processed using ImageQuant (GE Healthcare) and the protein level analysis was done with the DeCyder software (GE Healthcare). To detect phosphoproteins, 400 μg of HCC and non-HCC samples were separately run on 2-DE gels and stained with ProQ Diamond (Invitrogen). After acquiring images, gels were counterstained with SYPRO Ruby to visualize total proteins as described above.

Protein identification. The excised protein spots were in-gel digested with porcine trypsin (Promega). For LC-ESI-IT MS/MS analysis using LCQ Deca XP (Thermo Electron), the digested and dried peptides were dissolved in 10 μl of 0.1% formic acid in 2% acetonitrile (ACN). The dissolved samples were loaded onto C18 silica gel capillary columns (Magic C18, 50 × 0.2 mm), and the elution from the column was directly connected through a sprayer to an ESI-IT MS. Mobile phase A was 2% ACN containing 0.1% formic acid, and mobile phase B was 90% ACN containing 0.1% formic acid. A linear gradient from 5% to 65% of concentration B was applied to elute peptides. The ESI-IT MS was operated in positive ion mode over the range of 350–2000 (m/z) and the database search was carried out against the IPI Human using MASCOT (Matrixscience). The following search parameters were used: the cutting enzyme, trypsin; one missed cleavage allowed, mass tolerance window, ±1 Da, the MS/MS tolerance window, ±0.8 Da; carbamidomethyl cystein and oxidized methionine as fixed and variable modifications, respectively.

Detection of phosphorylated peptide. Possible phosphorylation sites were investigated by MALDI–TOF–MS using monoammonium phosphate (MAP) added matrix mainly according to Nabetani et al. [21]. An additive of MAP was mixed with α-CHCA matrix solution (5 mg/mL, 0.1% TFA, 50% ACN aqueous) to 40 mM in final concentration. Tryptsin digests of the spots positively stained with ProQ were dissolved into 4 μL of 0.1% TFA, 50% ACN aqueous solution and 1 μL of the peptides solution was spotted on the MALDI target plate. After drying up, 1 μL of the MAP matrix was dropped on the dried peptide mixture. Voyager DE-STR (ABI) was used to obtain mass spectra both in negative and positive ion mode. MS peaks that had relatively stronger intensities in negative ion mode than in positive ion mode were selected as candidates for acidically modified peptides.

Results and discussion

We identified 195 spots representing 125 proteins (Suppl. Table 1) and obtained the corresponding mRNA expression data for a total of 93 proteins (149 spots) (Suppl. Table 2). These 93 proteins were classified according to their biological processes and subcellular localizations into categories described by the Gene Ontology Consortium (http://www.geneontology.org/index.shtml) and about a half of them were related to metabolic processes (Fig. 1A). It is a general agreement that proteins with extremely high or low p*I* as well as hydrophobic proteins are difficult to be detected by 2-DE. Being consistent with this notion, our analysis detected many cytoplasmic proteins (Fig. 1B). Therefore, the protein expression data presented here were biased in favor of cytoplasmic and soluble proteins. The protein expression abundance between non-HCC and HCC was calculated using the normalized spot volume, which was the ratio of spot volume relative to IS (Cy3:Cy2 or Cy5:Cy2) and we used the Student's paired *t*-test ($p < 0.05$) to select the protein spots which were expressed differentially between non-HCC and HCC, using 2-DE gel images run in triplicate. The spot volume of a multi-spotted protein was indicated as a total volume by integrating the intensities of multiple spots as was done by Gygi et al. [10]. Comparison of protein expression profiles revealed that several proteins were expressed differentially between HCC and non-HCC. Proteins whose abundances increased >2-fold or decreased <1/2 in HCC are listed in Table 2. While glutamine synthetase, vimentin, annexin A2 and aldo-keto reductase were up-regulated, carbonic anhydrase 2, argininosuccinate synthetase 1, carbonic anhydrase 1, fructose-1,6-bisphosphatase 1, and betaine-homocysteine methyltransferase were down-regulated in HCC. Up- or down-regulation of most of these proteins in HCC has been reported previously [22–27]. Up-regulation of vimentin and annexin A2, and reduced expression of carbonic anhydrase 1 and 2 was suspected to be associated with cellular motility and metastasis [23,24,26].

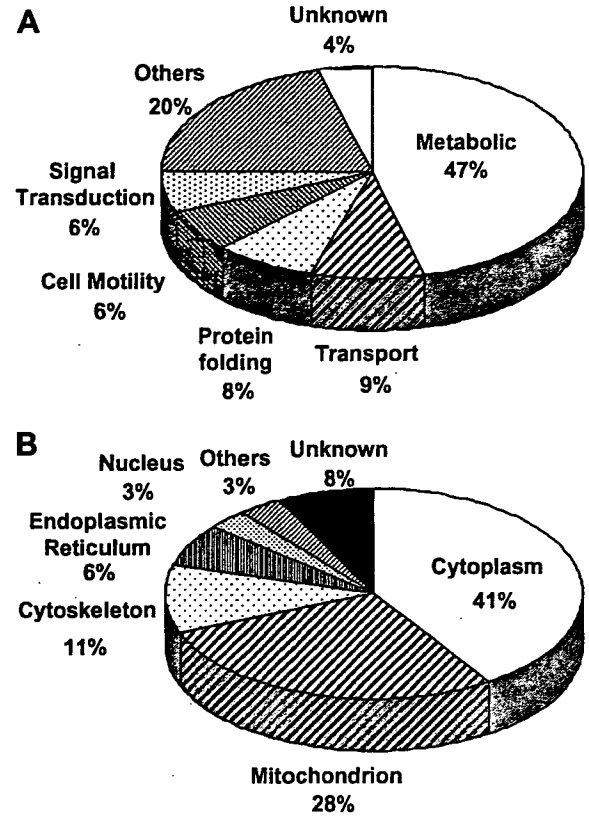

Fig. 1. Classification of identified proteins according to their cellular function (A) and subcellular localization (B).

The mRNA expression abundance was calculated from cDNA microarray data. Hierarchical clustering of

Table 2
Proteins expressed differentially between HCC and non-HCC

Spot ID	Protein name	Refseq ID	Theoretical		Fold change (HCC/non-HCC)		References
			p*I*	MW (kDa)	Protein[a]	mRNA	
1353, 1354	Glutamine synthase	NP_002056.2	6.43	42.7	2.06	3.08	[22]
1039, 1046	Vimentin	NP_003371	5.09	53.6	2.30	1.51	[23]
1716	Annexin A2	NP_001002857.1	7.57	38.8	2.57	1.82	[24]
1685, 1699	Aldo-keto reductase 1B10	NP_064695	7.12	36.2	4.29	4.73	[25]
1977	Carbonic anhydrase 2	NP_000058	6.87	29.3	0.39	0.62	[26]
1307, 1312, 1331	Argininosuccinate synthetase 1	NP_000041.2	8.08	46.8	0.41	0.30	[27]
1941	Carbonic anhydrase 1	NP_001729	6.59	28.9	0.47	1.25	[26]
1582	Fructose-1,6-bisphosphatase 1	NP_000498	6.54	37.2	0.48	0.36	
1256	Betaine-homocysteine methyltransferase	NP_001704	6.41	45.4	0.48	0.40	

[a] Integrated spot volume was used to calculate the fold change of multi-spotted proteins.

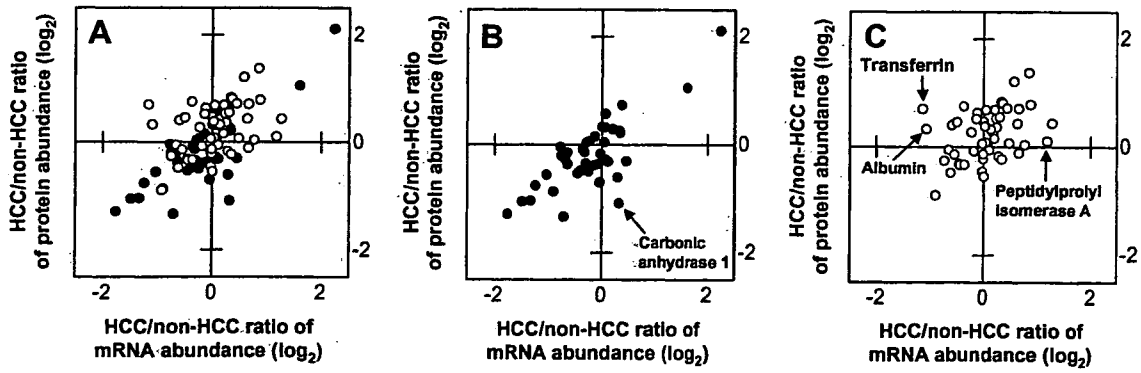

Fig. 2. Comparative analysis of protein and mRNA expression profiles between HCC and non-HCC. (A) The HCC/non-HCC ratios of averaged protein expression levels for 93 proteins were plotted against those of mRNA. Proteins related to metabolic pathways were indicated in closed circles and were shown again in (B). Proteins related to the other biochemical pathways were indicated in open circles and shown in (C). Proteins listed in Table 3 were indicated in (B) and (C). All graphs were depicted in $\log_2$ scale.

Table 3
Proteins whose expression changes between HCC and non-HCC show poor correlation to mRNA expression changes

Spot ID	Protein name	Refseq ID	Theoretical		Spot[a] Av. Ratio	Spot *p* value	Protein ratio	Micro array Av. ratio	Micro array *p* value
			*p*I	MW (kDa)					
564	Transferrin	NP_001054	6.8	79.3	2.23	0.035	1.61	0.45	3.3E−06
565					1.87	0.079			
566					2.28	0.13			
605					0.73	0.098			
1489	Albumin	NP_000468	5.9	71.3	—	0.63	1.25	0.47	2.3E−03
1941	Carbonic anhydrase 1	NP_001729	6.6	28.9	—	3.5E−03	0.47	1.25	0.39
2290	Peptidylprolyl isomerase A	NP_066953	7.7	18.1	—	5.0E−01	1.07	2.29	1.1E−01

[a] Since transferrin was detected in multiple spots, averaged ratio and spot *p* value of each spot is shown.

Table 4
Multi-spotted proteins showing spot-to-spot differences in expression level between non-HCC and HCC

Spot ID	Spot Av. ratio	Spot *p* value	Protein name	Refseq ID	Theoretical		Protein[a] ratio
					*p*I	MW (kDa)	
436	1.92	5.3E−04	Tumor rejection antigen (gp96)	NP_003290	4.8	92.7	1.2
537	0.79	0.16					
564	2.23	0.035	Transferrin	NP_001054	6.8	79.3	1.61
565	1.87	0.079					
566	2.28	0.13					
605	0.73	0.098					
1257	1.02	0.92	Fumarate hydratase	NP_000134	8.8	54.8	0.8
1261	0.6	1.3E−03					

[a] HCC/non-HCC protein ratios were calculated using integrated spot abundances.

gene expression was done with BRB-ArrayTools (http://linus.nci.nih.gov/BRB-ArrayTools.htm). The filtered data were log-transferred, normalized, centered, and applied to the average linkage clustering with centered correlation. BRB-ArrayTools contains a class comparison tool based on univariate *F* tests to find genes differentially expressed between predefined clinical groups. The permutation distribution of the *F* statistic, based on 2000 random permutations, was also used to confirm statistical significance. A *p* value of less than 0.05 for differences in HCC/non-HCC gene expression ratio was considered significant.

The average HCC/non-HCC expression ratios of the 93 proteins were plotted against the mRNA ratios in Fig. 2, where a positive value indicates increased expression in HCC and a negative ratio indicates reduced expression. The overall expression ratio of HCC/non-HCC indicated noticeable correlation between protein and mRNA

(Fig. 2A), and the Pearson's correlation coefficient for this data set (93 proteins/genes) was 0.73. Next, we divided 93 proteins into those related to metabolism and others biological processes. The HCC/non-HCC ratios of protein expression for metabolism-related proteins showed substantial correlation with those of mRNA (Fig. 2B, $r = 0.9$), whereas those of other proteins were poorly correlated (Fig. 2C, $r = 0.36$). Extreme care must be taken in a direct comparison of proteomic data with transcriptome because of multiple layers of discrepancies caused by the distinct sensitivities of cDNA array hybridization and 2-DE, the inability of a cDNA array to distinguish mRNA isoforms and post-translational modifications of proteins. Nevertheless, our results suggest that the expression of considerable portion of proteins with metabolic function listed here is regulated at transcriptional level. On the other hand, post-transcriptional and/or post-translational processes seem to be involved in the regulation of expression level for proteins with other cellular functions as a whole. Four proteins (albumin, transferrin, peptidylproryl isomerase A, and carbonic anhydrase 1) showed apparent poor correlation in protein and mRNA expression profiles (Table 3 and Fig. 2). Transcriptional control might have little effect on the expression changes of these proteins between HCC and non-HCC.

A number of proteins were expressed as multiple spots on 2-DE gels and most multi-spotted proteins showed little spot-to-spot variations in the averaged HCC/non-HCC ratio. Although we do not know how these multiple spots were generated, many of them might be due to the conformational equilibrium of proteins under electrophoresis rather than to any post-translational modifications [28]. On the other hand, the HCC/non-HCC expression ratios of several multi-spotted proteins varied from spot to spot, and three proteins (transferrin, fumarate hydratase, and tumor rejection antigen gp96) were categorized as these multi-spotted proteins (Table 4).

For example, gp96 was detected in two spots (spot #436 and 537) with distinct molecular mass and p*I* and they showed different HCC/non-HCC expression ratio (Fig. 3A and B and Table 4). The expression of these two isoforms was observed to change in the opposite direction between non-HCC and HCC: #436 was up-regulated in HCC (HCC/non-HCC ratio: 1.96) while #537 was down-regulated (HCC/non-HCC ratio: 0.79) (Table 4 and Fig. 3C and D). Gp96 is a glycoprotein present in endoplasmic reticulum and is supposed to function as a molec-

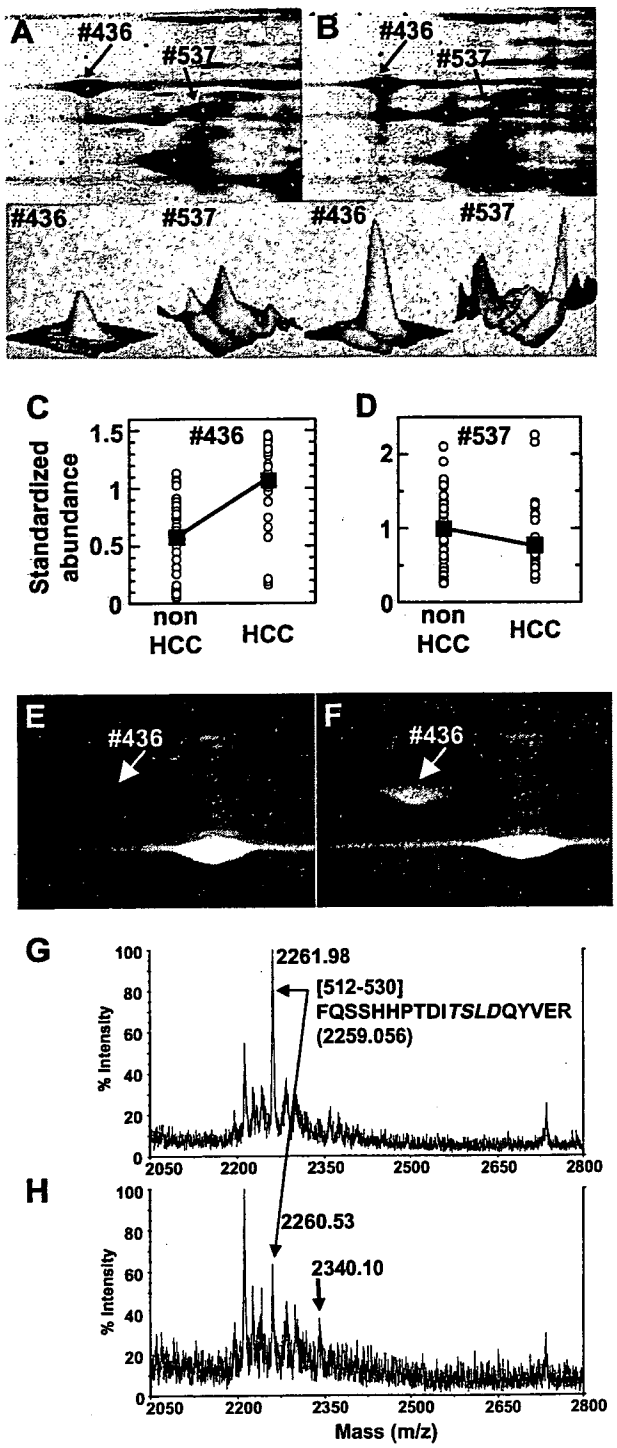

Fig. 3. Comparison of expression profiles of two gp96 spots between HCC and non-HCC. The expression profile and phosphorylation of tumor rejection antigen gp96 in HCC and non-HCC was investigated. Magnified gel images and 3D views of two gp96 spots in non-HCC (A) and HCC (B) were shown. Differences in expression level of two gp96 spots, #436 (C) and #537 (D), between non-HCC and HCC were shown. The open circle indicates the standardized abundance of the individual spot in each sample. The closed square represents the averaged abundance of each gp96 spot. Magnified gel images of non-HCC (E) and HCC (F) stained with ProQ. The #436 spot was positively stained with ProQ, while unambiguous staining of the #537 spot was not observed. Tryptic peptides prepared from the spot #436 were analyzed by MALDI–TOF mass-spectrometry in the positive ion mode (G) and the negative ion mode (H). A peak of 2261.98 detected in positive ion mode corresponds to the amino acid sequence from 512 to 530. In addition to the original peak (*m/z*: 2260.53), a peak mass shifted by +80 Da was detected in the negative ion mode. A predicted phosphorylation consensus motif for protein kinase CK2 is indicated in italics (G).

ular chaperone and intracellular Ca^{2+} regulator [29,30]. Several previous reports have shown that gp96 is glycosylated and phosphorylated, and exists as heterogeneous molecular entities with various molecular weights [31]. In order to know whether gp96 spots were phosphorylated or not, we stained the 2-DE gels with ProQ Diamond which is a dye specific to proteins phosphorylated on serine, threonine or tyrosine residues [32], and has been used successfully to visualize phosphoproteins [33]. We found that the spot #436 was positively stained with ProQ (Fig. 3E and F). We further tried to detect possible phosphorylated peptides in the tryptic digests prepared from #436 by MALDI–TOF–MS according to Nabetani et al. [21]. Searching for those peaks that had relatively stronger intensities in negative ion mode than in positive ion mode, we found two peaks as candidates for acidically modified peptides. They were assigned to the peptides SILFVPTSAPR (amino acid sequence: 385–395, data not shown) and FQSSHHPTDITSLDQYVER (aa512–530). Fig. 3G and H show the unmodified peak and the acidically modified peak (mass shifted by +80 Da in negative ion mode) of the latter peptide, respectively. This peptide contained a predicted phosphorylation consensus motif, [Ser or Thr]-X-X-[Asp or Glu], for protein kinase CK2 (Fig. 3G) which was suggested to phosphorylate gp96 [34]. These results together with ProQ staining indicated that at least one gp96 isoform was phosphorylated and was up-regulated in HCC. Over-expression of gp96 in HCC has been reported previously [35], though the reports that showed over-expression of its phosphorylated form are rare. Further investigation into biological meaning of gp96 phosphorylation may provide us important information about HCC development.

Acknowledgments

We thank the late Dr. A. Tsugita for helpful discussion through this work and N. Tetsura for technical assistance.

Appendix A. Supplementary data

Supplementary data associated with this article can be found, in the online version, at doi:10.1016/j.bbrc.2007.11.101.

References

[1] T.K. Seow, R.C.M.Y. Liang, C.K. Leow, M.C.M. Chung, Hepatocellular carcinoma: from bedside to proteomics, Proteomics 1 (2001) 1249–1263.
[2] L.J. Lopez, J.A. Marrero, Hepatocellular carcinoma, Curr. Opin. Gastroenterol. 3 (2004) 248–253.
[3] H.F. Kawai, S. Kaneko, M. Honda, Y. Shirota, K. Kobayashi, Alpha-fetoprotein-producing hepatoma cell lines share common expression profiles of genes in various categories demonstrated by cDNA microarray analysis, Hepatology 3 (2001) 676–691.
[4] N. Iizuka, M. Oka, H. Yamada-Okabe, N. Mori, T. Tamesa, T. Okada, N. Takemoto, K. Hashimoto, et al., Differential gene expression in distinct virologic types of hepatocellular carcinoma: association with liver cirrhosis, Oncogene 22 (2003) 3007–3014.
[5] T. Yamashita, S. Kaneko, S. Hashimoto, T. Sato, S. Nagai, N. Toyoda, T. Suzuki, K. Kobayashi, et al., Serial analysis of gene expression in chronic hepatitis C and hepatocellular carcinoma, Biochem. Biophys. Res. Commun. 282 (2001) 647–654.
[6] K. Kawaguchi, M. Honda, T. Yamashita, Y. Shirota, S. Kaneko, Differential gene alteration among hepatoma cell lines demonstrated by cDNA microarray-based comparative genomic hybridization, Biochem. Biophys. Res. Commun. 329 (2005) 370–380.
[7] Y. Midorikawa, M. Makuuchi, W. Tang, H. Aburatani, Microarray-based analysis for hepatocellular carcinoma: from gene expression profiling to new challenges, World J. Gastroenterol. 13 (2007) 1487–1492.
[8] N.A. Shackel, D. Seth, P.S. Haber, M.D. Gorrell, G.W. McCaughan, The hepatic transcriptome in human liver disease, Comp. Hepatol. 5 (6) (2006).
[9] T.J. Griffin, S.P. Gygi, T. Ideker, B. Rist, J. Eng, L. Hood, R. Aebersold, Complementary profiling of gene expression at the transcriptome and proteome levels in *Saccharomyces cerevisiae*, Mol. Cell. Proteomics 4 (2002) 323–333.
[10] S.P. Gygi, Y. Rochon, B.R. Franza, R. Aebersold, Correlation between protein and mRNA abundance in yeast, Mol. Cell. Biol. 19 (1999) 1720–1730.
[11] M. Unlu, M.E. Morgan, J.S. Minden, Difference gel electrophoresis: a single gel method for detecting changes in protein extracts, Electrophoresis 11 (1997) 2071–2077.
[12] I.N. Lee, C.H. Chen, J.C. Sheu, H.S. Lee, G.T. Huang, C.Y. Yu, F.J. Lu, L.P. Chow, Identification of human hepatocellular carcinoma-related biomarkers by two-dimensional difference gel electrophoresis and mass spectrometry, J. Proteome Res. 6 (2005) 2062–2069.
[13] C.R. Liang, C.K. Leow, J.C. Neo, G.S. Tan, S.L. Lo, J.W. Lim, T.K. Seow, P.B. Lai, et al., Proteome analysis of human hepatocellular carcinoma tissues by two-dimensional difference gel electrophoresis and mass spectrometry, Proteomics 5 (2005) 2258–2271.
[14] V.J. Desmet, M. Gerber, J.H. Hoofnagle, M. Manns, P.J. Scheuer, Classification of chronic hepatitis: diagnosis, grading and staging, Hepatology 19 (1994) 1513–1520.
[15] K.G. Ishak, P.P. Anthony, L.H. Sobin, Histological typing of tumours of the liver, 2nd ed.WHO International Histological Classification of Tumors, Springer-Verlag, New York, 1994.
[16] M. Honda, S. Kaneko, H. Kawai, Y. Shirota, K. Kobayashi, Differential gene expression between chronic hepatitis B and C hepatic lesion, Gastroenterology 120 (2001) 955–966.
[17] H.F. Kawai, S. Kaneko, M. Honda, Y. Shirota, K. Kobayashi, Alpha-fetoprotein-producing hepatoma cell lines share common expression profiles of genes in various categories demonstrated by cDNA microarray analysis, Hepatology 33 (2001) 676–691.
[18] M. Honda, H. Kawai, Y. Shirota, T. Yamashita, T. Takamura, S. Kaneko, cDNA microarray analysis of autoimmune hepatitis, primary biliary cirrhosis and consecutive disease manifestation, J. Autoimmun. 25 (2005) 133–140.
[19] M. Honda, T. Yamashita, T. Ueda, H. Takatori, R. Nishino, S. Kaneko, Different signaling pathways in the livers of patients with chronic hepatitis B or chronic hepatitis C, Hepatology 44 (2006) 1122–1138.
[20] Y. Tabuse, T. Nabetani, A. Tsugita, Proteomic analysis of protein expression profiles during *Caenorhabditis elegans* development using 2D-difference gel electrophores, Proteomics 5 (2005) 2876–2891.
[21] T. Nabetani, K. Miyazaki, Y. Tabuse, A. Tsugita, Analysis of acidic peptides with a matrix-assisted laser desorption/ionization mass spectrometry using positive and negative ion modes with additive monoammonium phosphate, Proteomics 6 (2006) 4456–4465.
[22] Y. Kuramitsu, T. Harada, M. Takashima, Y. Yokoyama, I. Hidaka, N. Iizuka, T. Toda, M. Fujimoto, et al., Increased expression and phosphorylation of liver glutamine synthetase in well-differentiated

hepatocellular carcinoma tissues from patients infected with hepatitis C virus, Electrophoresis 27 (2006) 1651–1658.
[23] L. Hu, S.H. Lau, C.H. Tzang, J.M. Wen, W. Wang, D. Xie, M. Huang, Y. Wang, et al., Association of Vimentin overexpression and hepatocellular carcinoma metastasis, Oncogene 23 (2004) 298–302.
[24] Z. Dai, Y.K. Liu, J.F. Cui, H.L. Shen, J. Chen, R.X. Sun, Y. Zhang, X.W. Zhou, Identification and analysis of altered alpha1,6-fucosylated glycoproteins associated with hepatocellular carcinoma metastasis, Proteomics 6 (2006) 5857–5867.
[25] E. Zeindl-Eberhart, S. Haraida, S. Liebmann, P.R. Jungblut, S. Lamer, D. Mayer, G. Jäger, S. Chung, H.M. Rabes, Detection and identification of tumor-associated protein variants in human hepatocellular carcinomas, Hepatology 39 (2004) 540–549.
[26] W.H. Kuo, W.L. Chiang, S.F. Yang, K.T. Yeh, C.M. Yeh, Y.S. Hsieh, S.C. Chu, The differential expression of cytosolic carbonic anhydrase in human hepatocellular carcinoma, Life Sci. 73 (2003) 2211–2223.
[27] P.N. Cheng, T.L. Lam, W.M. Lam, S.M. Tsui, A.W. Cheng, W.H. Lo, Y.C. Leung, Pegylated recombinant human arginase (rhArgpeg5,000mw) inhibits the in vitro and in vivo proliferation of human hepatocellular carcinoma through arginine depletion, Cancer Res. 67 (2007) 309–317.
[28] F.S. Berven, O.A. Karisen, J.C. Murrell, H.B. Jensen, Multiple polypeptide forms observed in two-dimensional gels of Methylococcus capsulatus (Bath) polypeptides are generated during the separation procedure, Electrophoresis 24 (2003) 757–761.
[29] J. Melnick, S. Aviel, Y. Argon, The endoplasmic reticulum stress protein GRP94, in addition to BiP, associates with unassembled immunoglobulin chains, J. Biol. Chem. 267 (1992) 21303–21306.
[30] H. Liu, E. Miller, B. van de Water, J.L. Stevens, Endoplasmic reticulum stress proteins block oxidant-induced Ca^{2+} increases and cell death, J. Biol. Chem. 273 (1998) 12858–12862.
[31] A.M. Feldweg, P.K. Srivastava, Molecular heterogeneity of tumor rejection antigen/heat shock protein GP96, Int. J. Cancer 63 (1995) 310–314.
[32] T.H. Steinberg, B.J. Agnew, K.R. Gee, W.-Y. Leung, T. Goodman, B. Schulenberg, J. Hendrickson, J.M. Beechem, R.P. Haugland, W.F. Patton, Global quantitative phosphoprotein analysis using multiplexed proteomics technology, Proteomics 3 (2003) 1128–1144.
[33] B.R. Chitteti, Z. Peng, Proteome and phosphoproteome dynamic change during cell dedifferentiation in Arabidopsis, Proteomics 7 (2007) 1473–1500.
[34] S.E. Cala, GRP94 hyperglycosylation and phosphorylation in Sf21 cells, Biochim. Biophys. Acta 1496 (2000) 296–310.
[35] D.F. Yao, X.H. Wu, X.Q. Su, M. Yao, W. Wu, L.W. Qiu, L. Zou, X.Y. Meng, Abnormal expression of HSP gp96 associated with HBV replication in human hepatocellular carcinoma, Hepatobiliary Pancreat. Dis. Int. 5 (2006) 381–386.

ELSEVIER

Journal of Hepatology 46 (2007) 26–36

Journal of Hepatology

www.elsevier.com/locate/jhep

Serum-derived hepatitis C virus infectivity in interferon regulatory factor-7-suppressed human primary hepatocytes

Hussein H. Aly[1,2,3], Koichi Watashi[2], Makoto Hijikata[2], Hiroyasu Kaneko[2], Yasutugu Takada[1], Hiroto Egawa[1], Shinji Uemoto[1], Kunitada Shimotohno[2,*]

[1]*Graduate School of Medicine, Department of Transplant Surgery, Kyoto University Hospital, Kyoto, Japan*
[2]*Laboratory of Human Tumor Viruses, Institute of Virus Research, Kyoto University, Japan*
[3]*Hepatology Department, National Hepatology and Tropical Medicine Research Institute, Cairo, Egypt*

See Editorial, pages 1–5

***Background/Aims*: The development of an efficient in vitro infection system for HCV is important in order to develop new anti-HCV strategy. Only Huh7 hepatocyte cell lines were shown to be infected with JFH-1 fulminant HCV-2a strain and its chimeras. Here we aimed to establish a primary hepatocyte cell line that could be infected by HCV particles from patients' sera.**

***Methods*: We transduced primary human hepatocytes with human telomerase reverse transcriptase together with human papilloma virus 18/E6E7 (HPV18/E6E7) genes or simian virus large T gene (SV40 T) to immortalize cells. We also established the HPV18/E6E7-immortalized hepatocytes in which interferon regulatory factor-7 was inactivated. Finally we analyzed HCV infectivity in these cells.**

***Results*: Even after prolonged culture HPV18/E6E7-immortalized hepatocytes exhibited hepatocyte functions and marker expression and were more prone to HCV infection than SV40 T-immortalized hepatocytes. The susceptibility of HPV18/E6E7-immortalized hepatocytes to HCV infection was further improved, in particular, by impairing signaling through interferon regulatory factor-7.**

***Conclusions*: HPV18/E6E7-immortalized hepatocytes are useful for the analysis of HCV infection, anti-HCV innate immune response, and screening of antiviral agents with a variety of HCV strains.**

***Keywords*: Immortalization; Primary hepatocytes; HCV infection; IRF-7; IRF-3; HPV18/E6E7; Innate immune response**

1. Introduction

Infection with Hepatitis C virus (HCV) is a serious problem worldwide since 3% of the world's population is chronically infected [1]. Chronic HCV may lead to liver cirrhosis and hepatocellular carcinoma. Current standard therapy utilizes the combination of pegylated interferon-α and ribavirin, which results in a sustained response in only 30–60% of patients [2–5]. Many patients, however, do not qualify for or tolerate standard therapy [6]. Thus, it is important to develop an efficient in vitro infection system for HCV to facilitate the discovery of new anti-HCV strategies. Only Huh7 cell line is permissive for replication, infection and release of the fulminant hepatitis-derived HCV-2a (JFH-1) *strain* and its chimeric derivatives [7–9]. No other hepatocyte cell lines are able to support HCV replication efficiently.

Received 5 June 2006; received in revised form 24 July 2006; accepted 1 August 2006; available online 30 October 2006

* Corresponding author. Tel.: +81 75 751 4000; fax: +81 75 751 3998.

E-mail address: kshimoto@virus.kyoto-u.ac.jp (K. Shimotohno).

0168-8278/$32.00
doi:10.1016/j.jhep.2006.08.018

Normal human hepatocytes are the ideal system in which to study HCV infectivity. When cultured in vitro, however, they proliferate poorly and divide only a few times [10]. Continuous proliferation could be achieved however by introducing oncogenes, such as Simian virus large tumor antigen (SV40 T) [11]. This often resulted in tumor development [12] together with numerical (aneuploidy) and structural (aberrations) chromosome abnormalities [13]. The human papilloma virus E6E7 genes (HPV/E6E7) immortalized multiple cell types that were phenotypically and functionally similar to the parental cells [14–20]. As yet, no human hepatocytes have been immortalized with HPV18/E6E7.

We established a human primary non-neoplastic hepatocyte cell line transduced with the HPV18/E6E7 that retained primary hepatocyte characteristics even after prolonged culture, and were more prone to HCV infection than those cells immortalized with SV40 T antigen. We further improved the susceptibility of HPV18/E6E7-immortalized hepatocytes to HCV infectivity by impairing interferon regulatory factor-7 (IRF-7) expression. These cells are useful to assay infectivity of HCV strains other than JFH-1, HCV replication, innate immune system engagement of HCV, and screening of anti-HCV agents. This infection system using non-neoplastic cells also suggested that IRF-7 plays an important role in eliminating HCV infection.

2. Materials and methods

2.1. Cell cultures

We obtained the approval of the Ethical Committee of Kyoto University for the use of human hepatocytes and sera obtained from HCV-positive patients. Informed consent was obtained from both the hepatocyte donor and HCV-positive patients. Primary hepatocytes (P.H.) were cultured as described [21]. HeLa, 293, Huh-7.5, and PH5CH8 cells were cultured as previously described [22]. For three-dimensional (3D) cultures, Mebiol Gel (Mebiol Inc.) was prepared according to the manufacturer's instructions.

2.2. Plasmids construction

The SV40 T, hTERT and HPV/E6E7 fragments from pAct-SVT, PCX4neo/hTERT, and pLXSN-E6E7 plasmids were inserted into pCSII-EF-RFA plasmid creating the pCSII-EF-SVT, pCSII-EF-hTERT, and pCSII-EF-E6E7 plasmids, respectively. The full-length IRF-3 and IRF-7 genes were cloned by RT-PCR using total RNA isolated from 293 cells as a template and were inserted into pcDNA3 vector. Dominant-negative forms of IRF-3 (DNIRF-3) and IRF-7 (DNIRF-7) were constructed by PCR amplification of the coding region for amino acid residues 108–427 of IRF-3 and 237-514 of IRF-7, respectively. The amplified IRF-3 fragment was cloned into pcDNA3 in frame with a FLAG epitope tag generating pcFLAG-DNIRF-3. The amplified IRF-7 fragment was cloned into pLXSH in frame with HA epitope tag generating pLXSH-HA-DNIRF-7. The pIFNβ promoter-luc and pIFNα promoter-luc plasmids were gifts from Dr. Taniguchi of the Tokyo University. The psiRNA-hIRF-3 and psiRNA-hIRF-7 plasmids were purchased from Invivogen (USA).

2.3. Immunoblot analysis

Immunoblot analysis was performed as described previously [22]. We used anti-SV40 T (Santa Cruz), anti-HPV18/E7 (Santa Cruz), anti-tubulin (Sigma), anti-FLAG (Sigma), and anti-HA (Sigma) antibodies.

2.4. Transfection, small interfering RNA silencing and luciferase assays

Transfection of plasmid DNA was performed using Effectene transfection reagent (Qiagen) as recommended by the manufacturer. The pLXSH-HA-DNIRF-7 plasmid was transfected into the HuS-E/2 clone; transfectants were selected in 100 μg/ml hygromycin B (Gibco). The psiRNA-hIRF-3 and psiRNA-hIRF-7 plasmids were separately transfected into HuS-E/2 cells followed by Zeocin (250 μg/ml) selection. After two weeks of continuous selection, cells were infected with HCV. Luciferase assays were conducted as previously described [22]. The results are presented as relative light units (RLU) normalized to the total content of protein in the cell lysates.

2.5. Reverse transcriptase polymerase chain reaction (RT-PCR) and real-time RT-PCR

Using 250 ng of total RNA as a template, we performed RT-PCR with a one-step RNA PCR kit (Takara) according to the manufacturer's instructions. The primer sets and reaction conditions used are detailed in Table 1. To measure HCV-RNA titers by real-time RT-PCR, we collected RNA from infected wells. Five hundred nanograms of total cellular RNA was analyzed for the quantity of HCV-RNA as previously described [23].

2.6. HCV infection experiment

HCV infection experiment from serum was done as mentioned before [22]. HCV-infected-serums were titrated and 1×10^5 HCV-RNA copies/ml were used for each infection experiment. Concentrated culture medium for HCV/JFH1-producing cells was prepared as previously described [7]. HCV titer in the concentrated medium was measured, adjusted and added to the cells as mentioned above.

2.7. Blocking of HCV infectivity by anti-CD81

Inhibition of HCV infectivity was performed by blocking CD81 as previously described [7].

3. Results

3.1. Establishment of immortalized primary human hepatocytes

Primary hepatocytes were isolated from liver tissue obtained from a 9-year-old male patient with Primary Hyperoxaluria who had undergone liver transplantation. Hepatocytes were left unmanipulated or transduced with CSII-EF-hTERT alone or in combination with CSII-EF-SVT or CSII-EF-E6E7 to enhance the efficiency of immortalization. After six weeks only cells transduced by the combination of hTERT and either LT or HPV18/E6E7 continued to proliferate. Initially appearing colonies with a growth advantage were picked up and expanded. SV40 T-immortalized cell clones were named HuS-T cells and given numbers from 1 to 7,

Table 1
Primer sequences and RT-PCR parameters

Genes	Primer sequence 5′–3′	PCR parameters[a]
HGF	F: AGGAGCCAGCCTGAATGATGA R: CCCTCTGATGTCCCAAGATTAGC	95, 56, 72 1 min, 45 s, 1 min
TGFα	F: ATGGTCCCCTCGGCTGGA R: GGCCTGCTTCTTCTGGCTGGCA	95, 59, 72 45 s, 30 s, 1 min
TGFβ1	F: GCCCTGGACACCAACTATTGCT R: AGGCTCCAAATGTAGGGGCAGG	95, 58, 72 45 s, 30 s, 1 min
TGFβ2	F: GATTTCCATCTACAAGACCACGAGGGACTTGC R: CAGCATCAGTTACATCGAAGGAGAGCCATTCG	95, 58, 72 45 s, 30 s, 1 min
HGFR	F: TGGTCCTTGGCGTCGTCCTC R: CTCATCATCAGCGTTATCTTC	95, 54, 72 30 s, 45 s, 1 min
EGFR	F: CTACCACCACTCTTTGAACTGGACCAAGG R: TCTATGCTCTCACCCCGTTCCAAGTATCG	95, 58, 72 45 s, 30 s, 1 min
TGFβ1R	F: CGTGCTGACATCTATGCAAT R: AGCTGCTCCATTGGCATAC	95 s, 54, 72 30 s, 45 s, 1 min
TGFβ2R	F: TGCACATCGTCCTGTGGAC R: GTCTCAAACTGCTCTGAAGTGTTC	95, 58, 72 45 s, 30 s, 1 min
FGFR	F: ATGTGGAGCTGGAAGTGCCTC R: GGTGTTATCTGTTTCTTTCTCC	95, 54, 72 30 s, 45 s, 1 min
IGF-1R	F: ACCCGGAGTACTTCAGCGCT R: CACAGAAGCTTCGTTGAGAA	95, 54, 72 30 s, 45 s, 1 min
HNF1α	F: GTGTCTACAACTGGTTTGCC R: TGTAGACACTGTCACTAAGG	95, 52, 72 45 s, 30 s, 1 min
HNF1β	F: GAAACAATGAGATCACTTCCTCC R: CTTTGTGCAATTGCCATGACTCC	95, 52, 72 1 m, 45 s, 1 min
HNF3β	F: CACCCTACGCCTTAACCAC R: GGTAGTAGGAGGTATCTGCGG	95, 56, 72 1 m, 45 s, 1 min
HNF4	F: CTGCTCGGAGCCACAAAGAGATCCATG R: ATCATCTGCCACGTGATGCTCTGCA	95, 58, 72 45 s, 30 s, 1 min
Albumin	F: AGTTTGCAGAAGTTTCCAAGTTAGTG R: AGGTCCGCCCTGTCATCAG	95, 55, 72 45 s, 30 s, 1 min
Apolipoprotein-a	F:AGGCTCGGCATTTCTGGCAG R: TATCCCAGAACTCCTGGGTC	95, 55, 72 45 s, 30 s, 1 min
HTF	F: TCGCTACAGCCTTTGCAATG R: TTGAGGGTACGGAGGAGTTCC	95, 55, 72 45 s, 30 s, 1 min
E-cadherin	F: TCCATTTCTTGGTCTACGCC R: TTTGTCCTACCGACTTCCAC	95, 55, 72 45 s, 30 s, 1 min
CYP 1B1	F: CACCAAGGCTGAGACAGTGA R: GCCAGGTAAACTCCAAGCAC	94, 57, 72 30 s, 30 s, 1 min
CYP 2C9	F: GGACAGAGACGACAAGCACA R: TGGTGGGGAGAAGGTCAAT	94, 57, 72 30 s, 30 s, 1 min
CYP 2B	F: GGCACACAGCCAAGTTTACA R: CCAGCAAAGAAGAGCGAGAG	94, 57, 72 30 s, 30 s, 1 min
CYP 3A4	F: TGTGCCTGAGAACACCAGAG R: GCAGAGGAGCCAAATCTACC	94, 57, 72 30 s, 30 s, 1 min
CYP 2E1	F: CCGCAAGCATTTTGACTACA R: GCTCCTTCACCCTTTCAGAC	94, 57, 72 30 s, 30 s, 1 min
CYP 1A1	F: AGGCTTTTACATCCCCAAGG R: GCAATGGTCTCACCGATACA	94, 57, 72 30 s, 30 s, 1 min
GAPDH	F: CCATGGAGAAGGCTGGGG R: CAAAGTTGTCATGGATGACC	95, 8, 72 45 s, 30 s, 1 min

Table 1 (*continued*)

Genes	Primer sequence 5′–3′	PCR parameters[a]
CD81	F: CTCAACTGTTGTGGCTCCAAC R: CCAATGAGGTACAGCTTCCC	95, 55, 72 45 s, 30 s, 1 min
TLR3	F: GATCTGTCTCATAATGGCTTG R: GACAGATTCCGAATGCTTGTG	95, 55, 72 45 s, 30 s, 1 min
TLR7	F: CCAGACATCTCCCCAGCGTC R: GGCAAAACAGTAGGGACGGC	95, 55, 72 45 s, 30 s, 1 min
TLR8	F: CTGTGAGTTATGCGCCGAAG R: CGGGATTTCCGTTCTGGTGC	95, 55, 72 45 s, 30 s, 1 min
Myd88	F: GGTCTCCTCCACATCCTCCC R: CCAGCTTGGTAAGCAGCTCG	95, 55, 72 45 s, 30 s, 1 min
IRF3	F: GAACCCCAAAGCCACGGATC R: CCTCCCGGGAACATATGCAC	95, 55, 72 45 s, 30 s, 1 min
IRF7	F: GTGCTGTTCGGAGAGTGGCTC R: CAGCCCAGGCCTTGAAGATG	95, 55, 72 45 s, 30 s, 1 min

CYP, cytochrome P450; EGFR, epidermal growth factor receptor; F, forward primer; FGFR, fibroblast growth factor receptor; GAPDH, glyceraldehyde phosphate dehydrogenase; HGF, hepatocyte growth factor; HGFR, hepatocyte growth factor receptor; HNF, hepatocyte nuclear factor; HTF, human transferrin; IGF-1R, insulin-like growth factor-type I receptor; IRF, interferon regulatory factor; R, reverse primer; TGF, transforming growth factor; TGFR, transforming growth factor receptor; TLR, toll like receptor.

[a] Temperatures are tabulated in the first lane in degrees celsius and the corresponding times in the second lane. Performing one-step RT-PCR, reverse transcription was carried out at 42 °C for 20 min with a pre-PCR denaturation at 95 °C for 10 min.

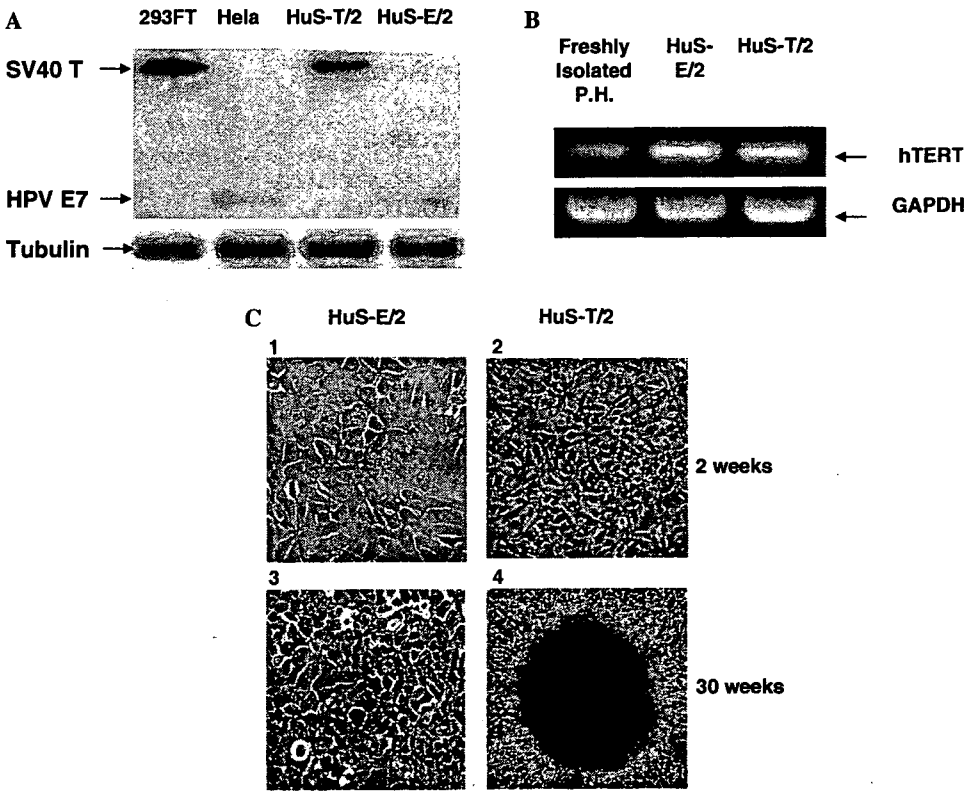

Fig. 1. (A) Immunoblot detection of SV40 T and HPV E7 expression in HuS-T/2 and HuS-E/2 cells, respectively. 293-FT and HeLa cells were used as positive controls for SV40 T and HPV E7 expression, respectively. The specific bands representing the targets are indicated. Detection of tubulin expression in all cells served as an internal control. (B) Human Telomerase Reverse Transcriptase (hTERT) expression was examined by RT-PCR in freshly isolated hepatocytes and the HuS-E/2 and HuS-T/2 cell lines. GAPDH expression was used as an internal control. The hTERT-specific bands are shown. (C) Morphological characteristics of HuS-E/2 and HuS-T/2 cells after two (panels 1 and 2) and 30 (panels 3 and 4) weeks in culture. [This figure appears in colour on the web.]